UNITED STATES DEPARTMENT OF THE INTERIOR

U.S. GEOLOGICAL SURVEY

Stretching of fluid inclusions in fluorite at confining pressures up to one kilobar

by

E. Lanier Rowan

Open-File Report 85-471

1985

CONTENTS

ILLUSTRATIONS

DEFINITION OF TERMS

Primary inclusions
: Inclusions trapped during crystal growth along growth planes.

Secondary inclusions
: Inclusions trapped during the healing of a fracture that formed after growth of the host crystal was complete. Planes of secondaries will cut across growth planes.

P_{ex}
: $P_{external}$; the pressure exerted either in nature or in the laboratory, on the crystal containing the inclusions.

P_{in}
: $P_{internal}$; pressure inside the inclusion (calculated).

T_H
: Homogenization temperature (also referred to in the literature as the filling temperature); in this study, the temperature at which the liquid has expanded to fill the entire cavity and the vapor completely dissolved in the liquid, leaving a single homogeneous phase. T_H represents a lower limit for the formation or trapping temperature of an inclusion.

Stretching
: An inelastic (i.e., permanent) deformation of the inclusion walls resulting in increased inclusion volume and therefore increased T_H. Stretching is the result of high internal pressure.

P_s
: $P_{stretch}$; the internal pressure required to initiate stretching in an inclusion.

T_s
: $T_{stretch}$; the temperature to which an inclusion must be heated to initiate stretching, i.e., the temperature required to produce P_s.

Overpressure
: $P_{in}-P_{ex}$; the difference between internal and external pressure, where $P_{in} \geq P_{ex}$. In this study, the values of interest are where $P_{in} \geq P_s$.

Overheating
: Heating an inclusion above its homogenization temperature.

T_{OH}
: $T_{overheating}$; temperature (°C) to which an inclusion has been heated, where $T_{OH} > T_H$.

INTRODUCTION

Fluid inclusions are widely studied for the information they provide on the formation conditions of their host minerals. The validity of the fluid inclusion data is based on a number of assumptions, the most fundamental of which are (1) that an inclusion is a closed system, and the total mass of its contents (liquid, solid, and gas) has remained constant since entrapment, and (2) that the cavity itself has not undergone deformation resulting in a permanent volume change. In other words, there has been neither movement of fluid into or out of the inclusion (leakage) nor deformation of the cavity (stretching). An understanding of the pressure-temperature (P-T) conditions that cause deformation as well as the ability to recognize deformed inclusions are important since leakage, and more recently stretching, have been reported in the literature. The purpose of this study therefore is to define the conditions under which stretching occurs in fluorite. Stretching has major implications in the study of mineral deposit genesis. Failure to recognize natural stretching may lead to serious misinterpretation of temperature data from inclusions and therefore of the formation temperature of their host mineral. Several stretching-related phenomena, "super-stretching," the entrapment of new (daughter) inclusions, and decreasing homogenization temperatures (T_Hs) at external pressures above 1 kilobar, also are discussed. These and other observations provide possible clues as to stretching mechanisms; currently both brittle failure and plastic deformation are proposed stretching mechanisms.

Leakage, described by a number of researchers (Ingerson, 1947; Kennedy, 1950; Lemmlein, 1956; Roedder and Skinner, 1968; and others), results from a high pressure gradient between the interior of the inclusion and the exterior of the crystal, and like stretching, causes an increased homogenization temperature (T_H). However, while stretching observed in this study was characterized by an absence of any optically visible fractures emanating from the inclusions, leakage is usually associated with visible cracks. Leakage may refer either to formation of a fracture extending to the surface, and emptying the inclusion of fluid, or to formation of a fracture which does not reach the surface, but increases the effective volume of the inclusion, thereby raising the T_H. Decrepitation, another widely used term, refers to the sudden, violent rupture of the inclusion walls due to high internal pressure. In the literature there is some overlap in usage between the terms stretching and leakage or partial leakage, and between leakage and partial decrepitation. In this study and in others (Larson et al., 1973; Roedder, 1981; Hollister, 1981; Bodnar and Bethke, 1984), stretching is defined as an inelastic (i.e., permanent) deformation of the inclusion walls due to high internal pressure, resulting in increased inclusion volume, vapor bubble volume, and T_H, without associated optically visible fractures in the host mineral. The term stretching is not intended to imply a mechanism, e.g., plastic deformation, or a directional expansion.

Larson and coworkers (1973) were among the first to discuss stretching as a phenomenon distinct from leakage. They reported essentially reproducible inclusion homogenization temperatures in fluorite and sphalerite ranging from 40°C to 70°C higher than the initial T_Hs due to inadvertent overheating in the laboratory. The vapor bubbles were described as visibly larger and only a few inclusions showed evidence of fractures. Subsequently, Bodnar and Bethke (1984) defined the relationships, in sphalerite and fluorite, between inclusion volume and P_s, the internal pressure required to initiate stretching, with external pressure, P_{ex}, constant at one atmosphere. As a

result of their study, usage of the term stretching in the literature is increasingly common (e.g. Roedder, 1981; Hollister, 1981). In fluorite, the P_s-volume relationship was defined as:

$$P_s = -147\text{Log}V + 900 \quad (1)$$

(Bodnar and Bethke, 1984, eq. 2), where P_s is in bars, and volume, V, is in cubic microns. As previous studies of stretching have not systematically examined the behavior of inclusions over a range of external pressures, the principal objective of the present study is to define the relationship between external pressure (P_{ex}), inclusion volume, and the temperature (T_s)/internal pressure (P_s) needed to induce stretching. The measurements made by Bodnar and Bethke (1984) have been combined with data from the present study (see Appendix B) and have been regressed to give the following equation:

$$P_s = -178.0\text{Log}V + 0.7P_{ex} = 1018.9 \quad (2)$$

where pressure (P) is in bars, and volume (V) is in cubic microns. External pressures ranged between 1 and 1034 bars and the temperatures reached in defining this relationship were below 300°C. As indicated by the negative and positive coefficients of LogV and P_{ex}, respectively, P_s has been found to increase with decreasing inclusion volume and with increased external pressure (figure 1). The overpressure (P_s-P_{ex}), however, appears to drop with increased external pressure suggesting a possible weakening of the fluorite. The P_s-P_{ex} relationship indicates that external pressure helps protect inclusions from stretching and, given independent estimates of post-trapping temperatures and pressures, makes possible evaluation of the likelihood that natural stretching has occurred.

Investigation of stretching at elevated external pressures is necessary to provide results applicable to a wide range of geologic conditions where stretching has, or is suspected to have occurred. While stretching, as a result of accidental overheating in the laboratory, has led to publication of misleading homogenization temperature data in the past (for example, Larson et al., 1973), this should no longer be a problem for most minerals now that the phenomenon is widely recognized. Natural stretching, however, remains a problem with serious potential implications. For example, a cycle of rising temperatures in a hydrothermal vein system could stretch inclusions trapped in early-stage, lower temperature minerals; regional, or more localized metamorphism resulting from intrusion of a pluton could raise temperatures sufficiently in a region to stretch inclusions in older, lower temperature minerals. In order to avoid misinterpretation, it must be possible for researchers to identify or at least make estimates as to whether or not stretching could have occurred. Bodnar and Bethke (1984) showed that the strong relationship between volume and P_s, documented in their study (figure 2) and in the present study (figure 1), may be used to identify a population of stretched inclusions, if enough inclusions spanning a broad enough size range are available. Since large inclusions stretch more readily than small ones, other factors being equal, any correlation between size and homogenization temperature is grounds for suspicion of stretching (figure 3a); a population of coeval unstretched inclusions will have T_Hs that show no relationship to volume (figure 3b). If, however, inclusions are sparse or relatively uniform in size, then an independently estimated post-entrapment maximum temperature and minimum pressure for the region are needed to give a reasonable evaluation of whether stretching has occurred.

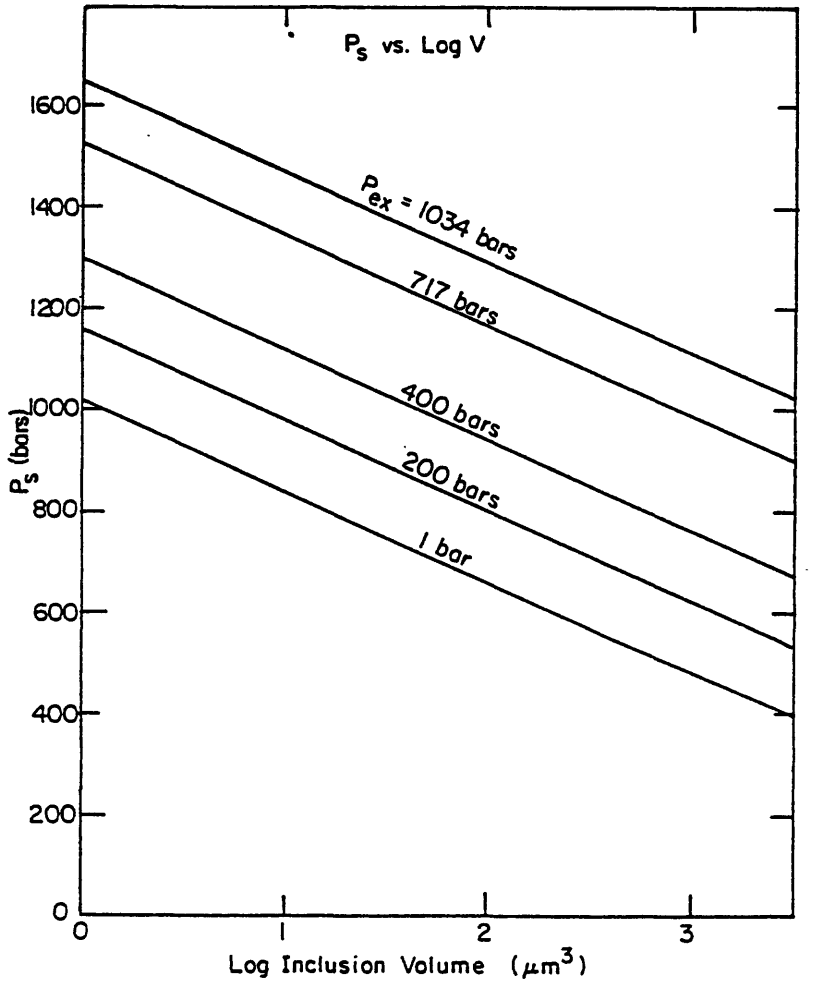

Figure 1. P_s vs. LogV at five external pressures

P_s vs. LogV curves have been drawn for each of the experimental external pressures used. The curves were plotted from equation (2) which was derived from regression of the entire data set (Appendix B):

$$P_s = -178.0\text{LogV} + 0.7P_{ex} + 1018.9$$

Within the pressure and volume range shown, P_s (the internal pressure required to initiate stretching), increases with increased P_{ex} (external pressure), and decreases with increased inclusion volume.

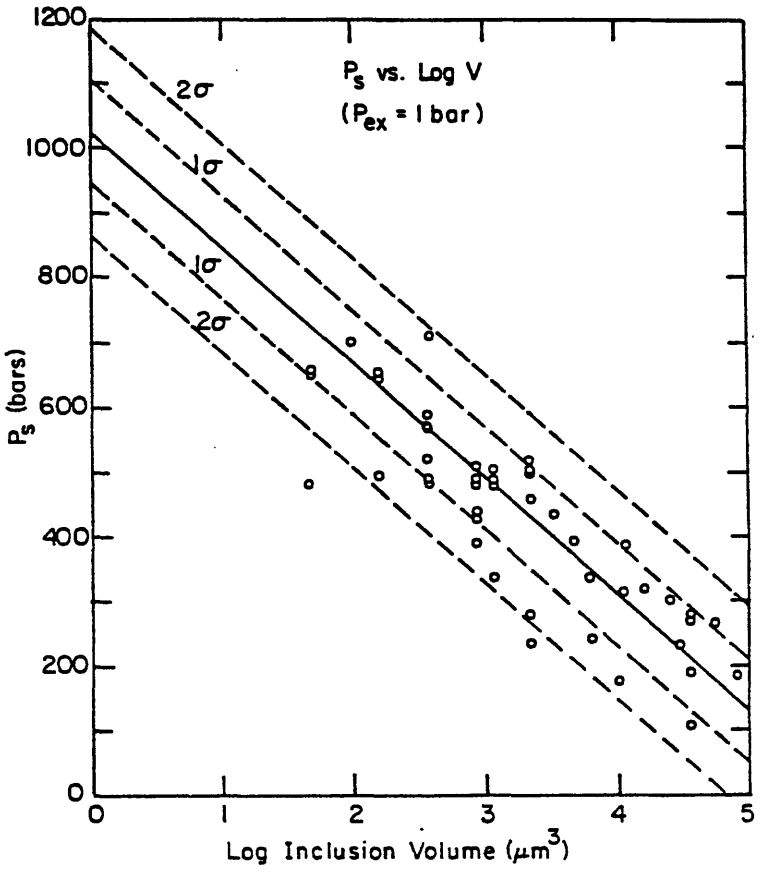

Figure 2. P_s vs. LogV at P_{ex}=1 bar

Data from the 45 inclusions tested by Bodnar and Bethke (1984) are plotted around the line derived from equation (2):

$$P_s = -178.0 \text{ LogV } + 0.7(1) + 1018.9$$

One standard deviation is 79.5 bars.

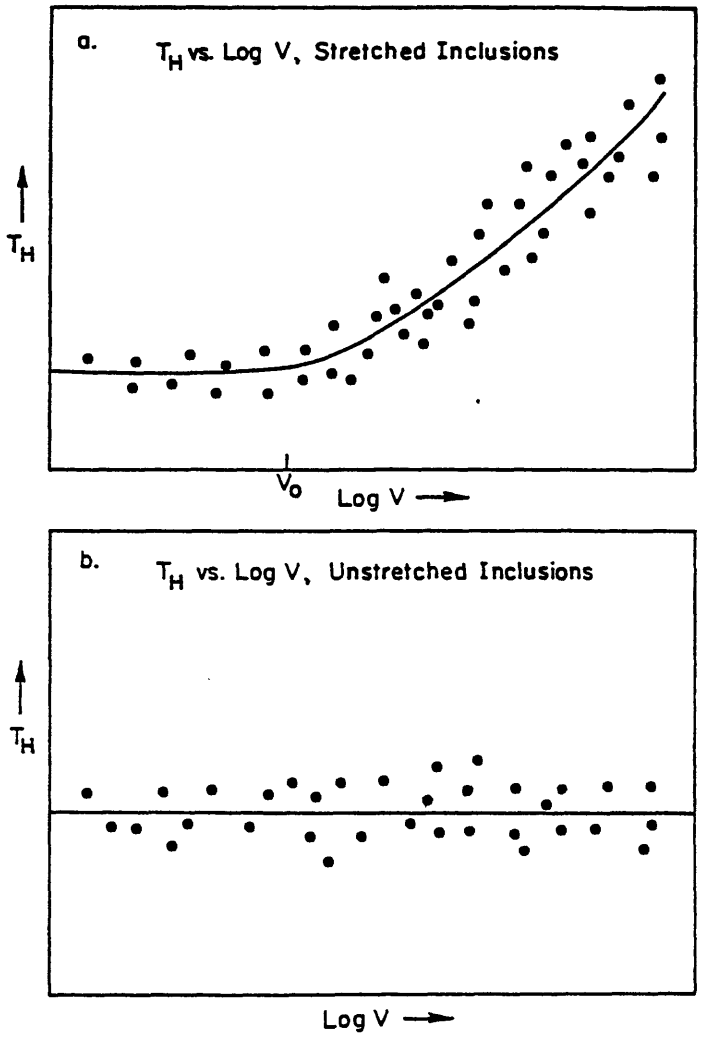

Figure 3. T_H vs. LogV: stretched and unstretched populations of inclusions (after Bodnar and Bethke, 1984, figure 9)

Fig. a. shows schematically a population of stretched inclusions. Inclusions below a certain minimum volume, V_0, have not been stretched, but above V_0, T_H increases with increased volume indicating that large inclusions have undergone a greater amount of stretching than smaller ones. The break in slope at V_0 defines the inclusion volume below which internal pressure was not great enough to induce stretching. Given a P_{ex} value, V_0 may be used to calculate P_s and the associated overheating temperature. Fig. b shows schematically the absence of any relationship between T_H and LogV indicating an unstretched population of inclusions.

DESCRIPTION OF EXPERIMENT

Introduction

The internal pressure needed to stretch the inclusion in this study was produced by heating the inclusions above their homogenization temperatures. The position in P-T space of a two-phase, liquid/vapor-bearing inclusion can be represented by points on a boiling curve up to the T_H (figure 4). In the inclusions used in this study, the last vapor dissolves in the liquid at the T_H, leaving a homogeneous liquid phase.

Somewhat less common are inclusions which when heated homogenize to a vapor phase. Liquid versus vapor phase homogenization can best be explained by a temperature-density diagram such as figure 5, which shows liquid-vapor phase relations for pure water. Salts in solution will commonly raise the two-phase boundary (solvus) without changing the overall geometry (Roedder, 1962b). In figure 5, two inclusions, A and B, are trapped at the same temperature, but at different pressures and fluid densities: 300 bars, 0.1 gm/cc and approximately 4500 bars, 0.7 gm/cc, respectively. The assumption of constant volume and mass, and therefore of constant density, requires that their cooling paths be vertically downwards. Each path crosses the two-phase boundary at the inclusion's homogenization temperature and density. Within the two-phase region, the lever rule is used to find the proportions of liquid and vapor. At 25°C, the lower density inclusion, A, contains predominantly vapor while B contains predominantly liquid. If the inclusions are reheated from room temperature, A will homogenize at the two-phase boundary and pass into the vapor field, eventually reaching its formation conditions in the supercritical region. Similarly, inclusion B will homogenize at the two-phase boundary, but will pass into the liquid field, and with increasing temperature will eventually reach its formation conditions. Homogenization to the liquid or vapor phase is determined by the location of the formation conditions on a diagram such as figure 5. An inclusion whose density is less than the critical density, 0.4 in this example, will homogenize to a vapor phase; if the density is greater than the critical density, homogenization will be to a liquid phase.

Returning to the pressure-temperature diagram (figure 4), further heating beyond T_H (overheating), causes the internal pressure to leave the boiling curve and rise rapidly along an isochore or isovolume curve whose slope is $(dP/dT)_v$ for the system. The formation temperature and pressure of an inclusion homogenizing to a liquid phase must lie at some point along this isochore, either on or above the liquid-vapor curve. The validity of assuming isochoric paths is discussed under Assumptions.

After a certain amount of overheating, the internal pressure reaches a critical value (P_s), above which stretching occurs, relieving stress from the cavity walls. Propagation of dislocations and the opening of submicroscopic fractures radiating out from the cavity walls are considered possible mechanisms for the apparent increase in inclusion volume. Since the increased pressure with temperature is substantially smaller for vapor than liquid, inclusions homogenizing to a vapor phase are far less likely to stretch, and are not discussed below. Stretching provides more space for expansion of the inclusion fluid and causes the T_H to rise. Stated another way, an increase in volume means that higher temperatures (i.e., higher T_Hs) must be reached in order for the liquid to expand to fill the entire cavity, given that an inclusion is a closed system with a fixed quantity (or mass) of fluid inside.

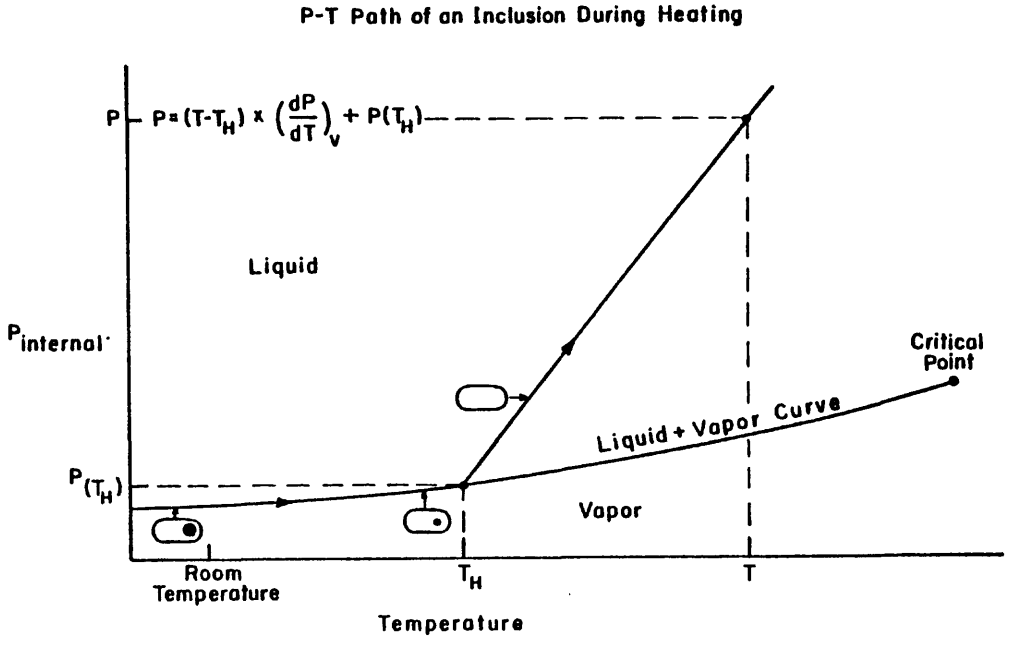

Figure 4. P-T path of an inclusion during heating

Schematic diagram showing a generalized liquid-vapor curve for the $NaCl-H_2O$ system with an isochore originating at the homogenization temperature, T_H. The vapor bubble, clearly visible at room temperature, decreases in size with heating, and vanishes at T_H leaving a single homogeneous liquid phase. With continued heating, pressure inside the inclusion rises rapidly along the isochore whose slope, $(dP/dT)_v$, is determined by the salinity of the fluid. At any temperature, T, above T_H, the corresponding pressure, P, is found as follows: $P = (T-T_H) \times (dP/dT)_v + P(T_H)$.

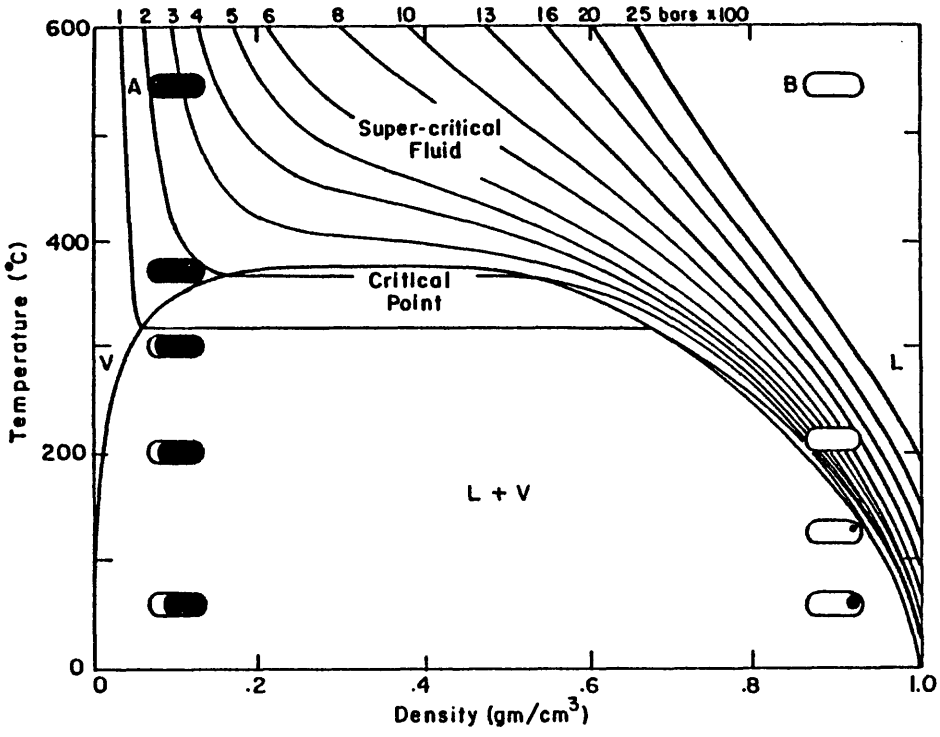

Temperature - Density Path of an Inclusion During Heating and Cooling

Figure 5. The temperature-density path of in inclusion during heating and cooling (from Roedder, 1962b)

Liquid and vapor phase relations are shown here for pure water, but the presence of dissolved salts will generally raise the two-phase boundary without changing the overall geometry of the diagram. The cooling path for inclusions trapped at A or B is vertically downward due to the assumption of constant inclusion volume, and therefore constant total fluid density. On heating, the inclusions homogenize at the boundary between the two-phase and the single phase regions.

At room temperature, the diameter of a vapor bubble in a stretched inclusion is increased, but since volume varies as the cube of radius, even significant volume increases are difficult to detect with an ocular micrometer. Larger volume increases resulting from prolonged stretching, however, have been measured. The increase in T_H of a stretched inclusion is the most noticeable and precisely measured effect of stretching. For this reason, stretching is referred to in terms of degrees of increase in the initial T_H rather than units of volume increase. For example, inclusions in this study will not generally show measurably increased vapor bubble diameters until stretched by several tens of degrees.

Sample material

The experiments were carried out on groups of secondary inclusions in late purple stage fluorite (Hall and Friedman, 1963; Cunningham and Van Heyl, 1980) from the Hill Mine, Cave-in-Rock district in southern Illinois. The polished sections made for this study were taken from the same samples used by Bodnar and Bethke (1984). Purple to clear color banding outlining growth planes facilitated distinction of primary, secondary, and pseudosecondary inclusions. Groups of 15 to 20 secondary inclusions were used because a relatively large number, spanning a broad volume range, were needed for statistically meaningful results. This precluded use of the far more scarce primary inclusions. In addition, the measurements become unreasonably time consuming unless the inclusions are all in one sample and grouped together so that they are easily located.

A major assumption in this study is that results drawn from the behavior of secondary inclusions can be generalized to primary inclusions. It has been suggested that the material in the rehealed fracture of a plane of secondaries may be weaker than the host mineral at some distance from the plane of secondaries, i.e., secondary inclusions might be more prone to stretching than isolated primary inclusions. It has also been argued, based on work by Gerlach and Heller (reported in Roedder and Skinner, 1968), that the material in a rehealed fracture may be stronger than the original mineral, meaning that secondaries would be less likely to stretch than primaries. Experiments with a limited number of primary inclusions (figures 6a and 6b), however, have yielded equivalent results at a 95% confidence level. Based on these results, primary and secondary inclusions in the temperature and pressure ranges of this study are assumed to behave the same with respect to deformation of the surrounding mineral.

Two other noteworthy points are the reported correlations of $P_{internal}$ required to deform an inclusion with inclusion shape and with depth from the sample surface. A number of researchers (Bodnar and Bethke, 1984; Leroy, 1979; Sharonov et al., 1973) have either observed or suggested that, if all conditions are equal, higher internal pressure is required to cause deformation (stretching, leakage, or decrepitation) in smooth-walled, sub-spherical inclusions than in irreguarlly shaped inclusions where stress concentrations can be localized at sharp 'corners.' For this reason, smooth-walled, sub-spherical morphology was one of the criteria for choosing inclusions for this study.

It has also been reported that the temperature and internal pressure required to cause deformation decreased with increased proximity to the sample surface (Shatagin, 1973; Pashkov and Piloyan, 1973). Roedder and Skinner (1968), in an investigation of the leakage phenomenon, suggested that inclusions lying within the near-surface zone of microfractures induced by grinding and polishing, might leak more readily than inclusions farther from the surface. They reported no relationship between leakage and distance from

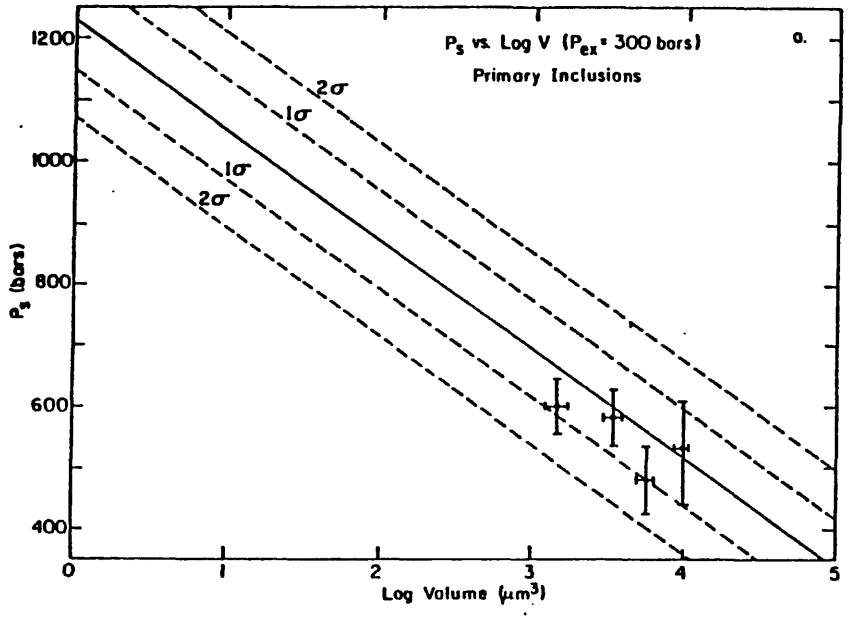

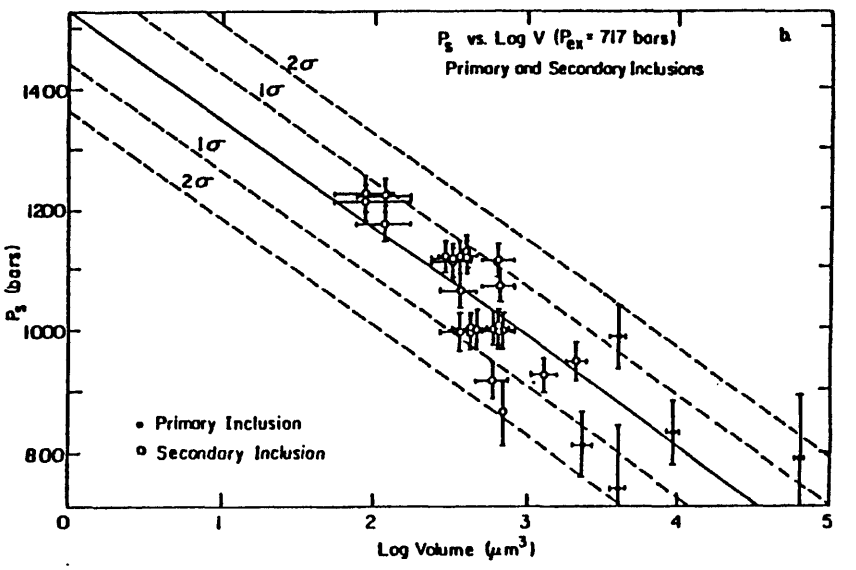

Figure 6. P_s vs. LogV: Comparison of primary and secondary inclusions

Fig. a. shows data from four primary inclusions (overheated at P_{ex}=300 bars) plotted around the line derived from equation (2),

$$P_s = -178.0\text{LogV} + 0.7(300) + 1018.9. \quad (2)$$

Equation (2) was derived by regression of all the experimental data gathered from secondary inclusions (Appendix B). One standard deviation is 79.5 bars. Fig. b. shows data from five primary inclusions (overheated at P_{ex}=717 bars) plotted around the regression line derived from equation (2),

$$P_s = -178.0\text{LogV} + 0.7(717) + 1018.9.$$

Data from 26 secondary inclusions overheated at the same external pressure are shown for comparison. At a 95% confidence level, the primary inclusions in Fig a. and Fig b. show the same P_s-LogV relationship as do the secondaries.

sample surfaces which, in their study, were not sawed, ground, or polished. They noted that inclusions in quartz as close as 5 microns to the surface did not leak under conditions where calculated internal pressure exceeded external pressure by 2-3 kbars. In the present study, a plot (figure 7) was made of P_s vs. depth below sample surface for 24 inclusions, and no P_s-depth relationship was found. In partucular, inclusions as close as 7 microns from sawed, ground, and polished surfaces showed no increased tendency to stretch.

Experimental method

The object of the experiment was to determine the temperature, T_s, at which stretching or deformation of the inclusion cavity began, and from T_s, to calculate the corresponding internal pressure, P_s. Doubly polished chips of fluorite containing inclusions were placed inside platinum capsules, which were loaded into cold-seal bombs attached to hydrothermal apparatus for control of external pressure, (P_{ex}). The platinum capsules, which were loosely crimped, protected the chips during loading, but allowed the pressure medium, water, to circulate freely around them. Argon was used instead of water for measurements made at an external pressure of 400 bars. The bombs were then placed in furnaces, and the chips were heated in increments of approximately ten degrees. The precision of furnace temperature and external pressure measurements were ±4°C and ±5 bars, respectively. Care was taken not to allow the calculated internal pressure to exceed the external pressure before the desired external pressure had been applied (figure 8). After each heating increment, the bomb containing the chip was cooled, the chip was removed, and each of the 20 to 30 inclusions was examined on a gas-flow heating/freezing stage (Werre et al., 1979) for changes in the T_H. The precision of a T_H measurement when the sample was removed from the stage and replaced was 1.5°C, and increases in T_H greater than 1.5°C were taken to indicate stretching. Each chip was heated in increments at a given P_{ex} at least until T_s, the temperature at which stretching began, had been bracketed.

Calculations

For the purpose of calculations, T_s was taken to be midway between the first temperature high enough to produce stretching and the previous overheating temperature below it; the error bar for T_s spans the entire interval (figure 9). Internal pressures in the inclusion were calculated from the P-V-T properties of the fluid with the assumption, discussed below, that the corrections due to fluorite solubility, thermal expansion, and elastic compressibility have small to negligible effects. Internal pressure above T_H, and before stretching has begun, is simply the amount of overheating, $T-T_H$, multiplied by the isochoric slope plus the vapor pressure at T_H (figure 4). When heated beyond a certain temperature, cooled and reheated, new T_Hs are observed (figure 10). The new T_H values are reproducible and have been found not to change until heated beyond the highest temperature previously reached.

At point A, the inclusion has just homogenized and the internal pressure is equal to the vapor pressure at that temperature. At point B, the inclusion has been heated to T_B and the internal pressure is $(T_B-T_{H-A}) \times (dP/dT)_V$ plus the vapor pressure, P_A. Point C and P_C are found in the same way and inclusions will homogenize at the initial temperature (T_{H-A}) until heated beyond T_C. When the inclusion is heated to T_D and cooled, a new T_H (T_{H-D}) is measured. The point at which stretching begins lies somewhere between C and D on figure 10; T_S, the temperature of initial stretching is bracketed by T_C and

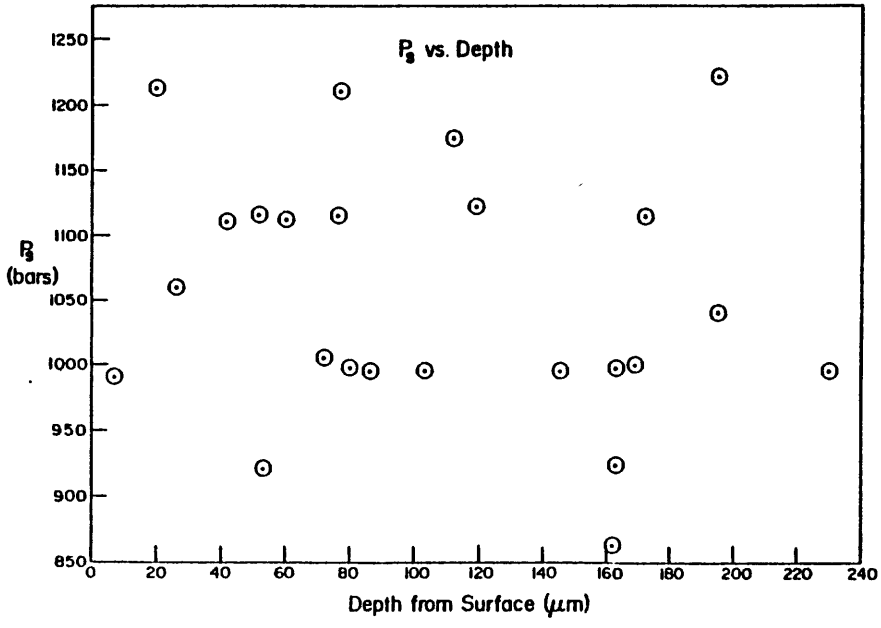

Figure 7. P_S vs. depth of inclusions from sample surface

The P_S values for 24 inclusions in sample 32, overheated at 717 bars external pressure, are plotted against the depth of each inclusion from the nearest sample surface. The graph shows no relationship between P_S and depth.

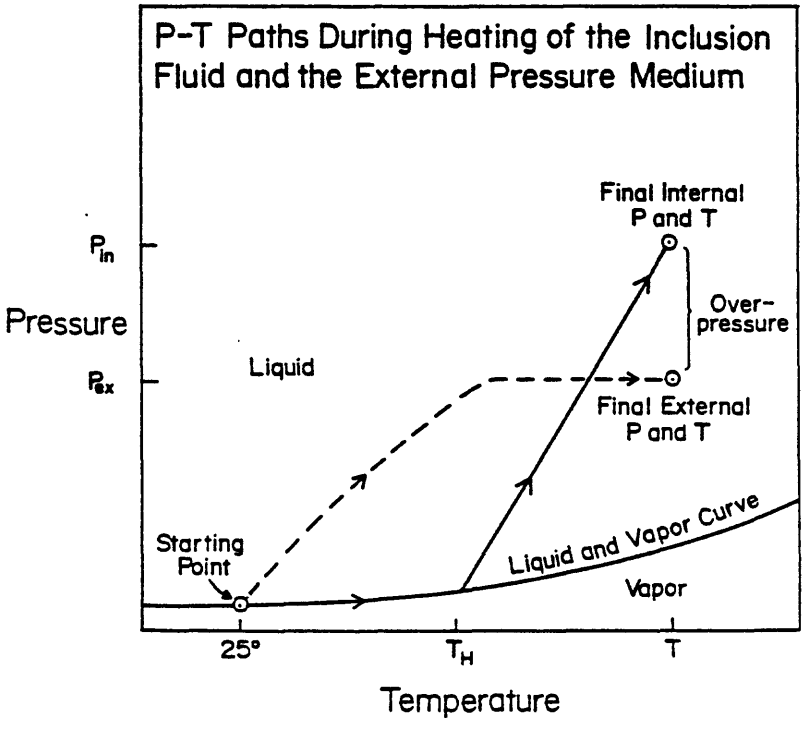

Figure 8. P-T paths during heating of the inclusion fluid and the external pressure medium

The solid line shows the P-T path followed by the inclusion fluid during heating, from the starting point, along the liquid-vapor curve to T_H, and then up the isochore to the final temperature, T, and corresponding internal pressure, P_{in}. The dashed line shows approximate P-T conditions outside the fluorite sample during heating. To prevent premature stretching, the external pressure was applied well before homogenization and the subsequent rapid internal pressure increase.

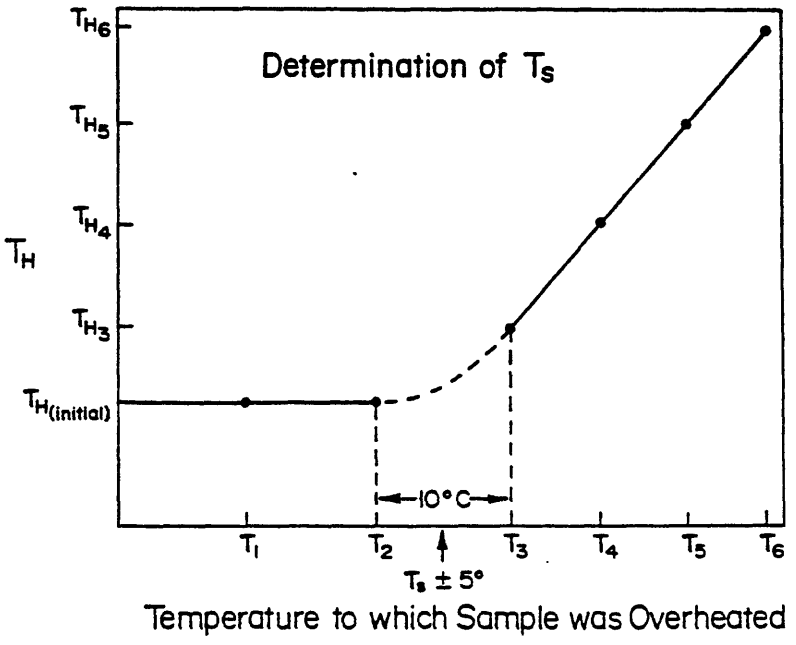

Figure 9. Determination of T_S

T_1 through T_6 are temperatures to which the fluorite sample was raised during incremental overheating. $T_{H(initial)}$ through T_{H6} are the corresponding new homogenization temperatures. T_S is taken to be the midpoint between T_2, the last overheating temperature to produce no change in $T_{H(initial)}$, and T_3, the first overheating temperature to raise $T_{H(initial)}$. The error bar spans the interval between T_2 and T_3.

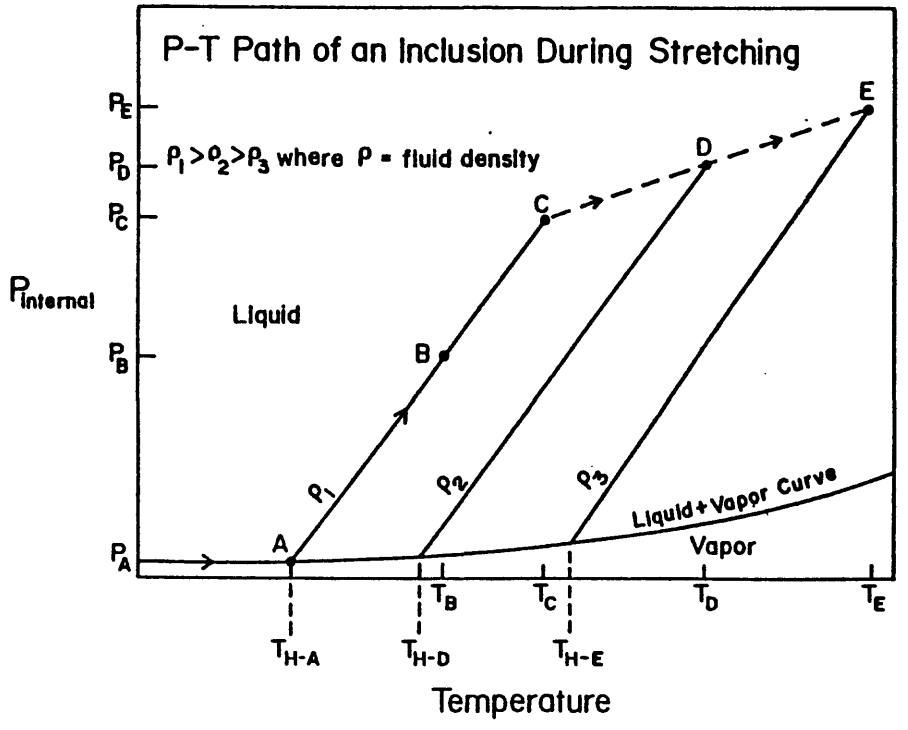

Figure 10. Schematic P-T path of and inclusion during stretching

The path of an inclusion along a generalized liquid-vapor curve and isochores in the NaCl-H_2O system are shown schematically. The inclusion homogenizes at A, and with heating passes through B, to C. When heated above T_C, the inclusion will stretch. Heating to T_D raises the initial T_H (T_{H-A}) to (T_{H-D}), and heating to T_E further raises T_H to T_{H-E}. The isochores are the constant volume/constant density cooling path followed by the inclusion fluid after each increment of overheating. The density of successive isochores decreases (specific volume increases) as stretching proceeds.

T_D. Given that the composition of the fluid and the isochoric slope are known, the point of intersection of an isochore originating at T_{H-D} with the overheating temperature, T_D, locates point D and the corresponding internal pressure, P_D. T_{H-D} will not increase until the inclusion is heated beyond T_D; when heated to T_E the homogenization temperature is raised to T_{H-E}.

The positions of A, B, and C were found in a very straightforward way; however, the position of D is based on the temperature to which the inclusion was heated, T_D, and the resulting new T_H (T_{H-D}) as well as isochoric slope. During initial heating, the inclusion's position in P-T space rises along the first isochore to C. Then, strictly speaking, the path between C and D travelled as T_D is first approahced, is unknown. On cooling and subsequent heating to T_D, the P-T path is along the isochore between the liquid-vapor curve and D. Reheating to, but not above, T_D does not change the T_{H-D}, indicating that the volume of the inclusion remains constant.

Isochores are P-T paths for inclusions which maintain essentially constant volume during overheating, and the shift to a new isochore represents an expansion in inclusion volume or stretching. Because of the lack of visible fractures associated with stretched inclusions, the important assumption is made that fluid has not escaped. The density of the fluid at the initial T_H and at all subsequent T_Hs can be calculated from data on the fluid density along the liquid-vapor curve. Again referring to figure 10, T_{H-A} remains constant until heated beyond T_C. At some temperature between T_C and T_D, the internal pressure exceeds the strength of the cavity walls and stretching takes place, increasing volume and decreasing the fluid density. At T_{H-D} the fluid has a new, lower density which is maintained on cooling and results in the increase in T_H to T_{H-D}. The densities along the different isochores can be used to find both absolute and relative inclusion volume changes that result from overheating. Absolute volume changes are found in two steps given an initial volume (see Appendix A):

(1) initial inclusion volume X fluid density at initial T_H = mass of fluid

(2) fluid mass X fluid's specific volume at new T_H = new inclusion volume.

NaCl equivalent salinities for the inclusion fluids were determined from freezing point depressions using the data of Potter, Clynne, and Brown (1978). Density data for the NaCl-H_2O system were taken from Potter and Brown (1977), and the liquid-vapor curve data were taken from Haas (1976). In most cases, P_s rather than T_s was used in plotting graphs. P_s makes possible comparison between inclusions of different salinities because it is calculated from the isochoric slope which varies with salinity; T_s, however, does not take into account the different salinities which ranged from 3.55 to 4.41 molal NaCl equivalent. The isochoric slopes ranged from 9 to 11 bars/°C, steepening with increased salinity in this temperature range.

Assumptions

Isochoric paths

In the calculation of P_{in}, the inclusion is assumed to follow an isochoric path in P-T space until permanent (i.e., inelastic) deformation occurs, increasing total inclusion volume. This constant volume assumption is valid only if the elastic volume changes, due to the thermal expansion of the crystal and compressibility with pressure are essentially negligible. The effect on inclusion volume of increased fluorite solubility with temperature

must also be taken into account. Thermal expansions were computed between a typical T_H (144°C) and the highest value of T_S (280°C) which was reached at the 1034 bar confining pressure. For this 'worst case' or maximum temperature range, the calculated volume expansions ranged from 1.38% (Ganesan and Srinivasan, 1959) to .894% (extrapolated from Skinner in Clark, 1966, p. 80), with an intermediate value for comparison of 1.033% extrapolated from synthetic fluorite data (Ballard et al., 1978). Until the initial inclusion volume determinations can be made with greater precision, the volume changes due to thermal expansion are assumed to be negligible.

Volume changes due to the compression of fluorite with increased pressure are found to be approximately an order of magnitude smaller than the volume changes due to thermal expansion. In calculating these volume changes, changes in the excess of internal over external pressure (i.e., net pressures) between T_H and T_S were used. Taking net pressure at T_H to be essentially zero, and 750 bars as the maximum net pressure at T_S (figure 11), volume changes of 0.105% (Vaidya et al., 1973), and 0.091% ± .001% (Bridgeman, 1925; Wong and Schuele, 1968; Brielles and Vidal, 1975) were calculated from bulk compressibilities expressed as functions of pressure at constant temperature. Because of good agreement in volume changes calculated from adiabatic (Vidal, 1974; Wong and Schuele, 1968) and isothermal (Bridgeman 1925; Vaidya et al., 1973) values, this distinction was ignored. To confirm that changes in bulk compressibility with temperature are of second order importance, a calculation was made using the adiabatic data of Vidal (1974) for a temperature increase from 25°C to 280°C. The resulting inclusion volume increase was 0.0025%. The increase in inclusion volume due to increased fluorite solubility between T_H and T_S is approximately three orders of magnitude smaller than the volume changes due to compressibility (Richardson and Holland, 1979). In light of the relatively small combined effects of solubility and elastic volume changes, isochoric paths have been assumed for the inclusions between T_H and T_S.

Salt content of fluids

The methods used to calculate inclusion volumes (Appendix A) and internal pressures in this study rely on knowledge of the fluid composition and its P-V-T properties. Although the inclusions in this study contain a complex brine, research discussed below has shown that thermodynamic properties of the brine are approximated well by those of a simple $NaCl-H_2O$ system. The fluids in primary inclusions from the late purple stage of Cave-in-Rock fluorite have been analyzed by Hall and Friedman (1963) and found to contain Na, K, Ca, Mg, Cl, and SO_4, with Na by far the most abundant cation (Hall and Friedman, 1963, Table 3). The procedure was to crush the samples in a vacuum line and condense the liberated water in a liquid nitrogen-cooled trap. Determination of the quantity of water in the inclusions is described by Hall and Friedman (1963), and a detailed description of the analytical methods used by them to identify and quantify the soluble salts present is given by Roedder, Ingram, and Hall (1963). The secondary inclusions used in this study are assumed to be very similar in composition to the primary inclusions based on relatively close agreement of their homogenization temperatures and freezing point depressions with those reported by Hall and Friedman (1963, Table 5) and Cunningham and Van Heyl (1980, Table 1) for primary inclusions of the same stage.

Measurement of freezing point depression is the generally accepted method of determining the total concentration of dissolved salts in the fluid phase

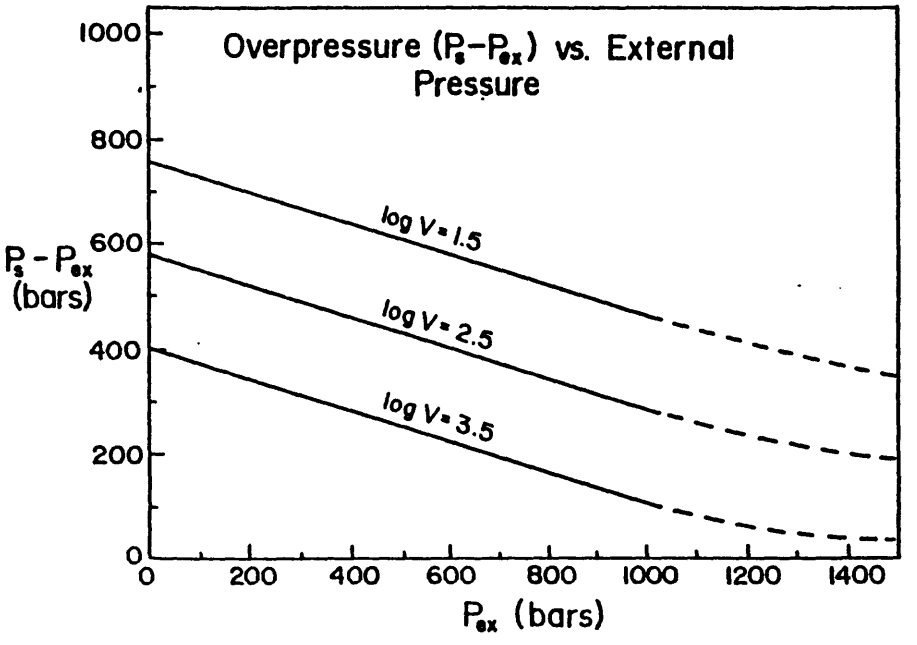

Figure 11. Overpressure (P_S-P_{ex}) vs. external pressure

The overpressure required to initiate stretching at a given inclusion volume is shown to decrease with increasing external pressure. The constant volume curves are derived from the equation (2),

$$P_S = -178.0\text{LogV} + 0.7P_{ex} + 1018.9.$$

Solid lines indicate the P_{ex} range of this study, and dashed lines show the speculative continuation beyond the upper, 1034 bar external pressure limit. The constant volume curves may approach the x-axis asymptotically.

of an inclusion (Roedder, 1962a; Hall and Friedman, 1963; Clynne and Potter, 1977). Experimental work by Potter and Clynne (1978) has shown that the P-V-T-X properties of brines in the system Na-K-Ca-Mg-Cl-Br-SO_4-H_2O can be predicted to within plus or minus 1% by the P-V-T properties of an NaCl solution with the same freezing point. A small correction is needed in the rare case where the ratios Ca/Na, K/Na, and Mg/Na exceed 0.5, 0.3, and 0.2, respectively (Potter and Clynne, 1978). Hall and Friedman (1963, Table 3), however, report ratios that fall well below these limits. Studies by Haas (1971) and Gibbard and Grossman (1974) provide additional evidence supporting the assumption that the P-V-T-X properties of an NaCl-H_2O system approximate well those of a more complex brine. In this study, therefore, the densities and isochoric slopes are calculated based on salinities reported as NaCl equivalents.

Gas content of fluids

Using the method described by Roedder (1970), several samples of the fluorite were crushed in an attempt to detect dissolved gas in the inclusions. Inclusion-bearing grains of fluorite the size of coarse sand were observed under a petrographic microscope while being crushed in kerosene between two glass plates. Kerosene is an excellent solvent for CH_4 and a relatively poor one for CO_2; it is therefore a good medium for identification of CH_4 versus CO_2. As fractures intersected inclusions, some of the vapor bubbles expanded, indicating that the precrushing internal pressure was, in these cases, greater than one atmoshpere. On contact with the kerosene, these bubbles dissolved very rapidly. This eliminated CO_2 as a possibility and strongly suggested methane, which has been reported in primary inclusions by Hall and Friedman (1963). Other inclusions contained no gas other than water vapor.

Because the crushing method operates on a group of small grains of the mineral, it is difficult to keep track of a given inclusion or plane of inclusions. The pressure of the glass plates introduces fractures randomly through the grains and randomly opens inclusions. Some of the crushed inclusions apparently contained methane, but observation of phases at room temperature and at low temperatures suggest that the specific planes of inclusions used in this study did not. The inclusions that contained either a solid phase or an immiscible fluid phase at room temperature were avoided, and those that did not were examined at low temperatures for the presence of CH_4 or other phases.

During initial freezing point depression measurements, the phases present at low temperatures were noted. Since super-cooling to -60°C to -70°C was usually necessary to nucleate ice crystals, further cooling to below -82.1°C the critical temperature for methane, was a simple procedure. Some of the inclusions used in the first runs were refrozen to check for dissolved methane; none was found. The relatively low critical pressure, 46.3 bars, means that at temperatures below -82.1°C methane should be visible as a liquid around the edges of the ice crystals, if it were present in a significant amount. Based on the absence of visible methane, the assumption has been made, for the purpose of calculations, that there was no methane in the specific planes of inclusions used. The effect of methane in the inclusions, however, would be to raise the liquid-vapor curve and steepen the slopes of the isochores (McGee et al., 1981; Susak and McGee, 1980), thereby shifting the P_s vs. LogV and Overpressure vs. P_{ex} curves upward, without changing their slope.

CO_2 is assumed to be absent from the inclusion fluid, again based on the lack of any observed additional phases, either at room temperature or below

-56.6°C, the triple point temperature. In addition, the results of crushing indicate that inclusions of other generations, and possibly of the same generation, do not contain CO_2. Finally, the presence of CO_2 has not been reported by Hall and Friedman (1963), Freas (1961), Cunningham and Van Heyl (1980), or by others who have studied fluid inclusions in Cave-in-Rock fluorites.

For the purpose of calculations, therefore, the only vapor or gas assumed to be present in the inclusions is water vapor.

DISCUSSION OF RESULTS

The P_{ex}-P_s Volume Relationship

Identification of stretched inclusions

Stretching may take place in nature when the inclusions in a mineral are subjected to higher temperatures and/or lower pressures than prevailed at the time of their formation. When internal pressure exceeds the combined external pressure and tensile strength of the mineral there is inelastic deformation of the cavity walls (Sabouraud, 1981). A number of references to stretching, leakage, or decrepitation due to overheating were mentioned earlier, but the release of external pressure may also induce deformation. An example of deformation due to pressure release would be the inclusion-bearing phenocrysts in nodules explosively transported to the surface through volcanic vents. Numerous CO_2-rich inclusions in olivine phenocrysts, many showing leakage or partial leakage, are described by Roedder (1965). The high external pressure at the time of their formation was equal to the pressure inside the inclusions, but as the nodules were brought to the surface, external pressure dropped and a steep pressure gradient between interior and exterior developed. It is this excess of internal over external pressure that causes deformation. While pressure imbalance resulting from elevated temperature (and hence increased internal pressure) has been the more commonly reported cause of deformation, a drop in external pressure below the level of internal pressure may have the same effect.

Measurements made by Bodnar and Bethke (1984) on 45 inclusions and by the author on 95 inclusions in fluorite have defined a relationship between external pressure, the volume of a fluid inclusion, and the maximum internal pressure that can be contained before the elastic limit of the inclusion walls is exceeded. The maximum internal pressure, P_s, was calculated from T_s as described earlier. Regression of the data (Appendix B) gave the following relationship:

$$P_s = -178.0\text{Log}V + 0.7P_{ex} + 1018.9 \qquad (2)$$

where pressure (P) is in bars, and volume (V) in cubic microns. The standard deviation of 79.5 bars and the multiple correlation coefficient 0.97. In this study, P_{ex} ranges from 1 to 1034 bars, and temperatures of initial stretching were below 280°C. Figure 1 summarized graphically the results of the regression.

If the composition of a fluid inclusion is known and the P-V-T data are available, then the above relationship can be used to draw certain conclusions about the likelihood that the inclusion had stretched. For a sample of fluorite containing inclusions with a size range of LogV between 1 and 3, the lowest internal pressure capable of stretching this population would be

expressed, based on equation (2) as:

$$P_s = -178.0(3) + 0.7P_{ex} + 1018.9 = .7P_{ex} + 485.0. \quad (3)$$

This relationship states that a minimum P_s of 485.7 bars (standard deviation = 79.5 bars) at P_{ex} = 1 bar, is needed to stretch the largest (LogV = 3) inclusions in this population. Any knowledge of P_{ex} such as an estimated minimum burial depth would place further constraints on P_s. A burial depth of 1 km, for example, would correspond to a lithostatic confining pressure of approximately 262 bars (Kennedy, 1950) or a hydrostatic pressure of 177 bars (Freas, 1961). Using this information, the equation is reduced to $P_s \geq 610$ bars assuming only hydrostatic pressure, or $P_s \geq 670$ bars assuming only lithostatic pressure. Thus, inclusions of specified volume, LogV = 3 in the example, would have stretched, if subjected to temperatures sufficient to raise their internal pressures above 610 bars, given a hydrostatic external pressure equivalent to a depth of 1 km. For inclusions such as those in the present study, homogenizing close to 145°C and containing fluids of approximately 20 weight percent NaCl equivalent, an internal pressure of 610 bars is generated by approximately 60°C of overheating to temperatures slightly over 200°C.

The final step is to 'test' individual inclusions for possible stretching, i.e., determine whether the temperatures reached were sufficiently high to cause stretching. For this an independent estimate is needed of the maximum post-trapping temperatures reached, based, for example, on diagenetic or metamorphic phase assemblages, or on the T_Hs of secondary inclusions. Referring to figure 12, P_s is the threshold internal pressure above which stretching will take place in inclusions larger than a given volume, and T_{max} is the highest temperature to which the inclusions were subjected during their post-formational history. Given a knowledge of the fluid composition and its P-V-T properties, the liquid-vapor curve and isochores originating from any point along it may be drawn. For an inclusion homogenizing at either A, B, or C, further overheating to T_{max} raises the internal pressure along the isochore to a point above the P_s. Inclusions with these observed T_Hs would have stretched, if heated to T_{max}. However, an inclusion homgenizing above D at E, F, and G could not have stretched because its internal pressure, if heated to T_{max}, would be below P_s. This testing method assumes that the path of an inclusion in P-T space during stretching is similar to the one shown in figure 13, in that volume does not increase enough to cause internal pressure to drop below P_s. The method breaks down if "super-stretching," discussed in the next section, has taken place. Super-stretching is seen as a sudden, large increase in T_H, indicating a volume increase possibly great enough to drop P_{in} below P_s. In these experiments, super-stretching occurred at overheating temperatures greater than 140°C above the T_Hs and was, in most cases, clearly recognizable. In the absence of super-stretching, a crude estimate of original T_H and therefore amount of stretching can be made based on the general geometry of the stretching path in P-T space (figure 13). The stretching determination method also relies on the fact that each new T_H resulting from overheating and stretching is reproducible until the inclusion is overheated to a still higher temperature. Reproducibility of a T_H indicates that no volume change has occurred in the laboratory.

The inclusions in fluorite from Saint Laurent-les-Bains studied by Sabouraud (1981) are examples of natural stretching which might lend themselves to this type of stretching analysis. The 296 inclusions from this region fell into two groups. At room temperature the majority were single phase liquid inclusions believed to have been trapped at low temperature ($\leq$50°C), while a few were two-phase, liquid-vapor inclusions which homogenized

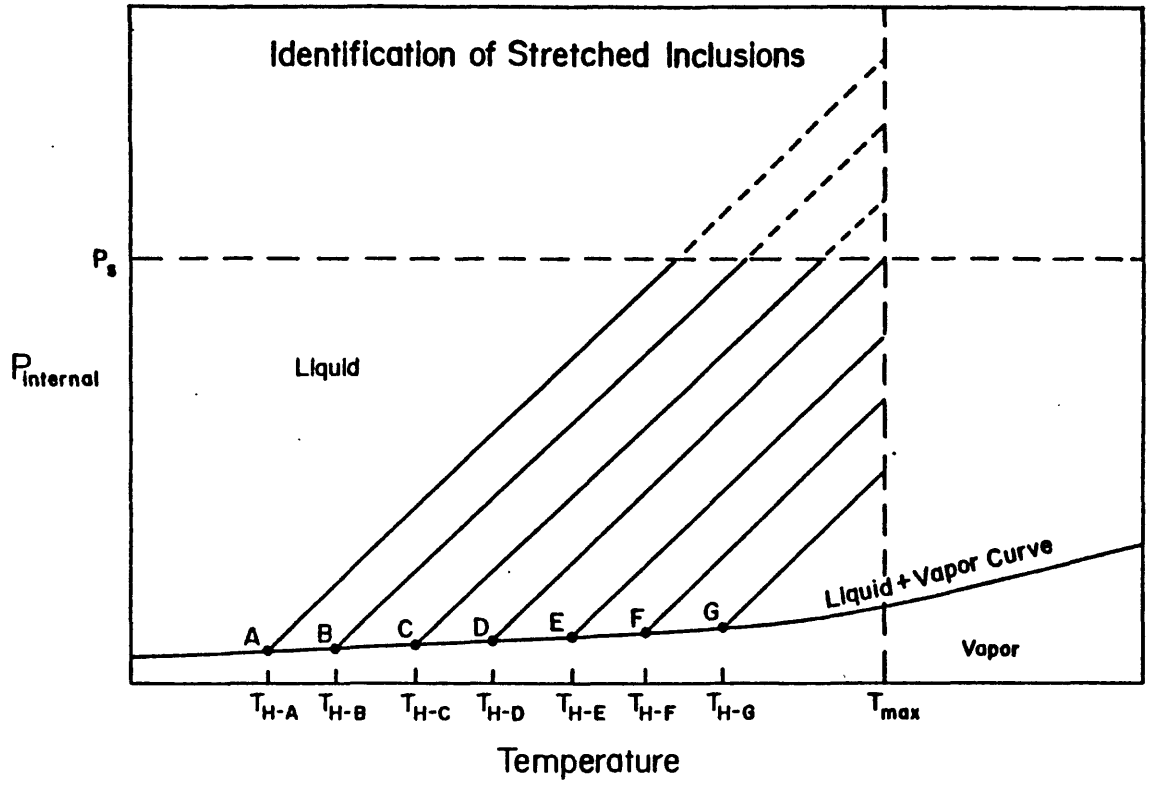

Figure 12. Identification of stretched inclusions

An inclusion of given volume homogenizing at T_{H-A}, T_{H-B}, or T_{H-C} would have stretched if heated to T_{max} because its internal pressure P_{in} would have exceeded P_s. P_s is a function of inclusion volume, and the external pressure during overheating; it could be calculated from equation (2),

$$P_s = -178.0\text{Log}V = +0.7P_{ex} + 1018.9.$$

An inclusion homogenizing at T_{H-E}, T_{H-F}, or T_{H-G}, would not have raised P_{in} above P_s.

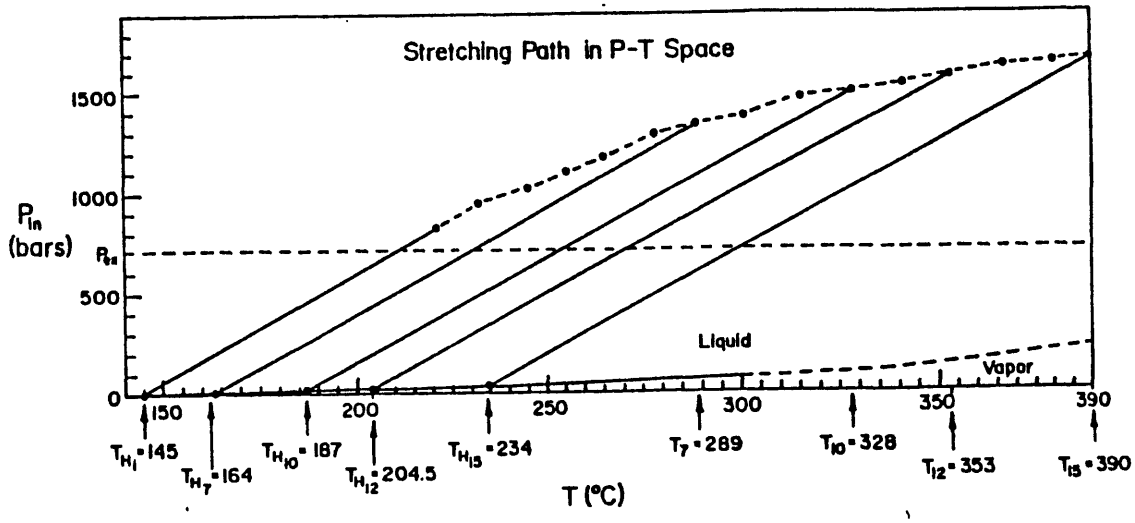

Figure 13. Stretching path in P-T space

As represented schematically in figure 10, the inclusion's internal pressure increases rapidly at first with increased temperature, then more slowly as stretching begins. The dashed line shows the stretching path followed by inclusion 32-a overheated at P_{ex}=717 bars. T_{Hi} is the initial T_H and each numbered T_H value (e.g. $T_{H\ 10}$=187°C) is the result of overheating to the indicated temperature (e.g. T_{10}=328°C). For this inclusion, LogV = 3.33, and salinity is 20.51 weight % or 4.414 molal NaCl equivalent, giving an isochoric slope of 10.5 bars/°C.

between 120°C and 180°C. The interpretation is that subsequent to trapping, the low-temperature primary inclusions were reheated to temperatures sufficient to stretch some, but not all of them. If the initial T_H were below 25°C (pressure correction at the time of trapping not taken into account), then a sufficient volume increase would lower the fluid density to the point where a vapor bubble could nucleate (see figure 5). The two-phase inclusions are described as showing no visible fracturing under the optical microcope. Although no correlation between volume and T_H was reported, a P_s-volume relationship of the type shown in figure 2 remains a possible explanation for the range in T_H values and the fact that not every inclusion was affected.

Figure 14 shows schematically one way in which the results of the present study might be used, in this case to estimate the amount of overheating that was needed to stretch the inclusions described by Sabouraud to their present homogenization temperatures. First an estimated confining pressure is needed to compute P_s for a given inclusion volume. Then with an estimate of initial T_H, a stretching path can be approximated and the overheating temperature bracketed as shown. Although more information is needed to complete the analysis, this example illustrates how a temperature of diagenesis might be determined.

Possible stretching mechanisms

Continued overheating beyond the initial temperature needed to stretch an inclusion results in an upward stretching path in P-T space (figure 13). The isochores on these diagrams are the cooling paths following each increment of heating and correspond to successively lower fluid densities or increased specific volumes. The relatively smooth increase in volume with temperature (figure 15) and with internal pressure (figure 16) suggests plastic deformation of the inclusion walls. Transmission Electron Microscope (TEM) photos of unheated fluorite samples showed approximately 10^8 dislocations per square cm, some of them intersecting inclusion walls (G. Nord, pers. comm., 1981), and it is thought that pressure on the cavity walls may supply the energy needed to activate these dislocations. Propagation of dislocations away from the inclusion into the crystal and possibly to the surface, may physically transport material away from the cavity walls, thus enlarging the inclusion. This mechanism, as well as an alternate, has been proposed by Bodnar and Bethke (1984). They suggest that the volume increases in this phase of stretching might also be caused by the opening of minute fractures in the cavity walls and their propagation into the crystal. No fractures are visible under the microscope, however, at 625X at room temperature, or at 512X at the homogenization temperatures of the inclusions.

The results of the present study and of work by Bodnar and Bethke (1984) show that the internal pressure required to stretch a given inclusion depends both on external pressure and inclusion volume. Although internal pressure at initial stretching always exceeded external pressure, this overpressure (P_s-P_{ex}) was less at higher internal pressures (see figure 11). This might be interpreted as a weakening of the fluorite with increasing temperature since at higher P_{ex}, P_s and therefore T_s is higher.

It is not currently understood why inclusions of large volume stretch at lower internal pressures than small ones, but if it is accepted that dislocations are involved in the stretching process, an analogy may be drawn between failure of the inclusion walls and failure of the walls of a circular tunnel in an underground mine. A tunnel of small diameter will stay open at far greater depth and lithostatic pressure than a tunnel of large diameter.

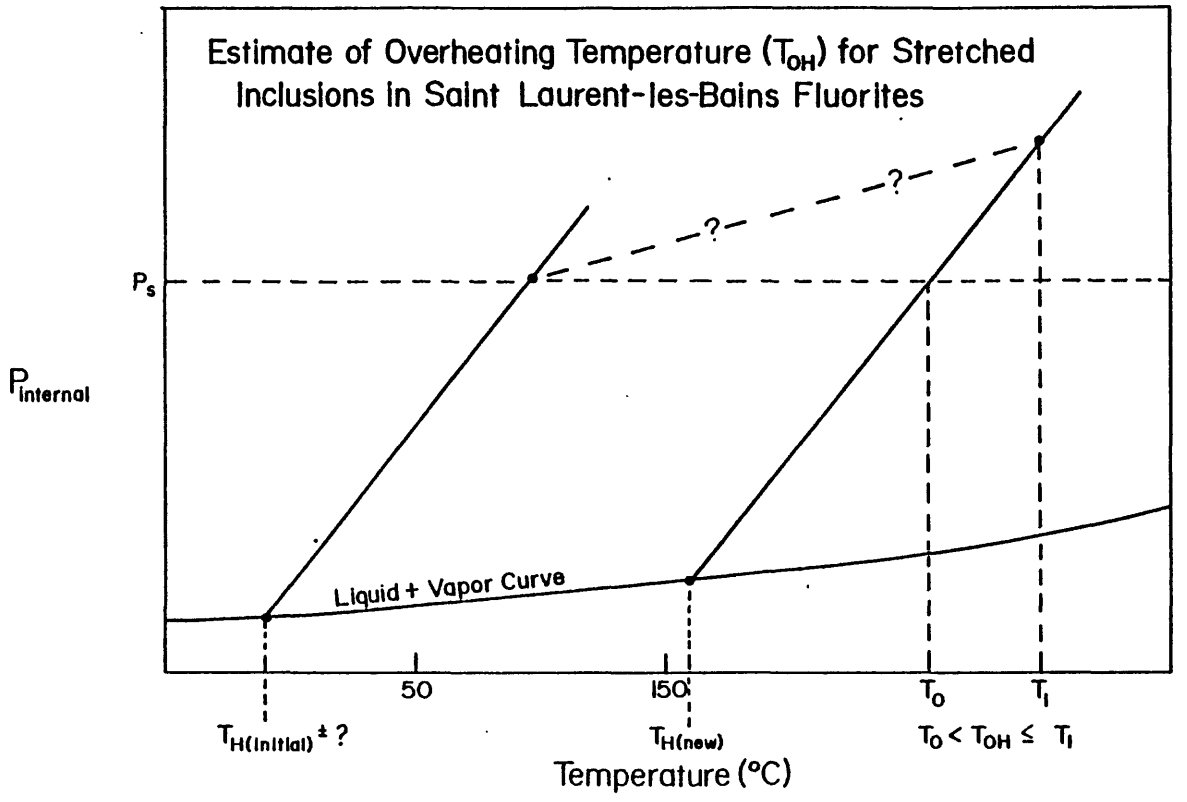

Figure 14. Estimate of overheating temperature (T_{OH}) for stretched inclusions in Saint Laurent-les-Bains fluorites

P_S is calculated from inclusion volume and from estimates of external pressure during overheating. $T_{H(new)}$, 160°C, is measured, and $T_{H(initial)}$ is known to be $\leq$50°C (see text). Isochores originating at the initial and new homogenization temperatures can be drawn given a fluid composition and a crudely approximated stretching path can be sketched between them. The intersection of the stretching path with the isochore originating at the new T_H, 160°C, defines an overheating temperature and corresponding pressure. Given that a stretching path has positive slope (figure 13), the overheating temperature is estimated to be between T_0 and T_1, or $T_0 < T_{OH} \leq T_1$ as shown.

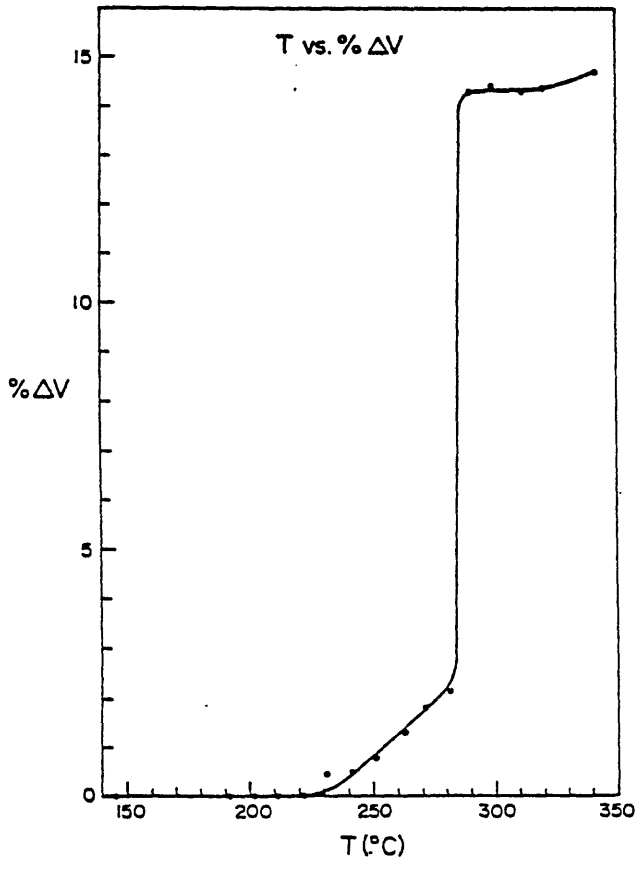

Figure 15. Temperature vs. % volume change for a super-stretched inclusion

The path shown is for inclusion 10A-c, overheated at 400 bars external pressure. T is the temperature to which the sample was raised during overheating; the % change in volume is computed from the decreased density (increased specific volume) of the inclusion fluid with increased T_H as a result of stretching (see figure 10). Figures 17 and 19 show the P-T path and changes in T_H for inclusions 10A-c and 10A-a, respectively, during super-stretching. During initial overheating between 145° and 221°C stretching has not yet begun and there is no increase in inclusion volume. This stage corresponds to the upward path along the initial isochore between points A and C in figure 10. Between 221° and 281°C 'normal' stretching occurs (points C through E in figure 10), and between 281° and 290° the inclusion super-stretches as indicated by the abrupt, and large increase in volume. After the super-stretching phase, volume continues to increase slowly. The inclusion's salinity was 4.18 molal or 19.62 weight % NaCl equivalent, giving an isochoric slope of 10.3 bars/°C; $T_{H(initial)}$ was 145°C and log inclusion volume $(microns)^3$, 2.95.

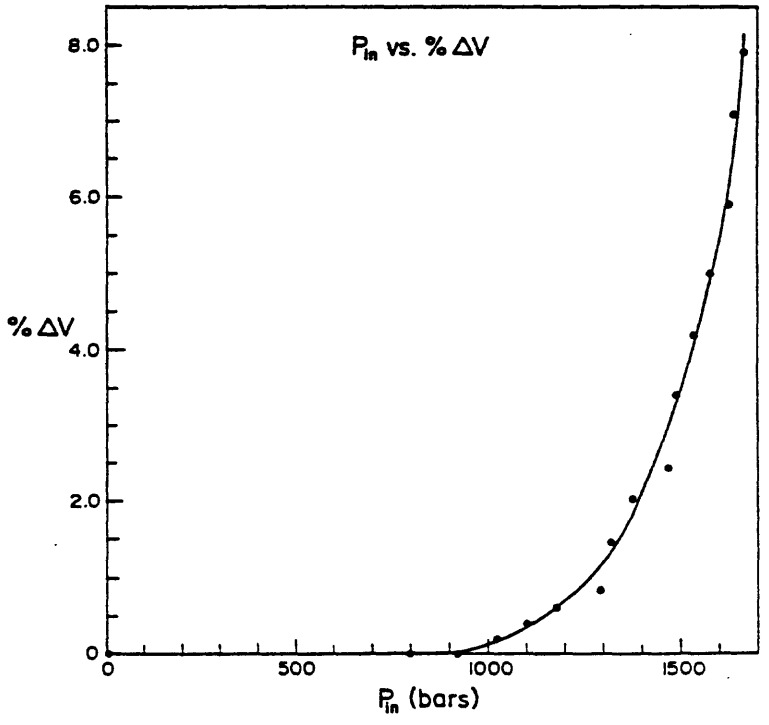

Figure 16. $P_{internal}$ vs. % volume change

Pressure inside inclusion 32-a, P_{in}, is plotted against the % increase in inclusion volume as a result of stretching. Below 919 bars stretching has not begun and there is no change in inclusion volume. Pressures above 919 bars cause stretching and a relatively smooth increase in inclusion volume. Compare with figure 18 which shows P_{in} vs. % volume change for a super-stretched inclusion. Inclusion 32-a, overheated at 717 bars external pressure, had a salinity of 4.414 molal or 20.51 weight % NaCl equivalent, giving an isochoric slope of 10.5/°C; $T_{H(initial)}$ was 145°C and log inclusion volume, 3.33.

Although the stress concentration around the tunnel and strength of the wall material is the same in both cases, the larger diameter tunnel will fail under a smaller load because it will intersect a greater number of the fractures, joints, and planes of weakness that are randomly distributed throughout the rock (M. Hood, pers. comm., 1982). As mentioned above there is a certain ambient density of dislocations in a fluorite cyrstal, and a large inclusion will be more likely to intersect one or more dislocations than will a small inclusion. If initial stretching does take place by propagation of dislocations, then it would seem logical for the inclusions whose walls intersected more dislocations to stretch (yield) at lower internal pressures.

When overheating was continued at the 400, 717, and 1034 bar confining pressures, the P-T paths of 18 inclusions turned downward (for example, figure 17). The pressure drop indicates a sudden increase in volume (figure 18) believed to represent a stretching mechanism different from the initial, postulated plastic deformation. A sharp increase in T_H and discontinuity in the T_H vs. overheating curve (figure 19) are evidence of the sudden volume increase. At the 717 and 1034 bar external pressures, this "super-stretching" phenomenon was accompanied by the appearance of scores of much smaller, new (daughter) inclusions which surrounded but did not touch the original parent inclusions (figure 20). At 200 bars external pressure, overheating was not extended into the temperature range where super-stretching might have occurred. At 400 bars external pressure, only two inclusions super-stretched and no new (daughter) inclusions were trapped. The daughter inclusions lie in the plane of the parent inclusions, and at 625X a distinct vapor bubble and faint inclusion outline can just be distinguished; they are too small to recognize homogenization, however. It has been suggested that the concentration of stress in the plane of the secondaries (parent inclusions), as they are stretching, causes a fracture to open and then heal rapidly on cooling, trapping new inclusions. It should be noted that any fractures formed during overheating had healed and were no longer visible when examined under the microscope. Since the runs in which new inclusions appeared were quenched in water at room temperature, the cooling time and therefore the time during which the hypothesized fracture healed was on the order of minutes. The fluid in the new inclusions presumably leaked from the parent inclusions, thereby explaining their sudden, large increase in T_H. Similar halos of tiny, daughter inclusions have been reported around inclusions known to have stretched either in nature or in the laboratory (Lemmlein, 1956, figures 6a,b and 7; Roedder, 1965, figure 18).

Upper external pressure limit

Figure 21 shows the increase of P_s with increased P_{ex} for a given volume, as defined by the regression equation. Below the 'limiting line' along with $P_{in}=P_{ex}$ (slope of 1.0), the external pressure exceeds internal pressure, and stretching, at least in the sense defined in this study, cannot take place. The curve LogV=0 is extrapolated from the regression equation and is interpreted as a theoretical maximum tensile strength for fluorite over a range of external pressures. An inclusion of LogV=0 is analogous to a tunnel of essentially zero diameter in the discussion above. The slopes of less than one appear to indicate diminishing mineral strength with increased external pressure, possibly as the result of the increased temperature (T_s) needed to generate P_s. Increasing temperature is implicit in increasing P_s and the two are related by the isochoric slope $(dP/dT)_v$ for a specific fluid composition. Clearly the $P_s=P_{ex}$-LogV relationship defined for the pressure,

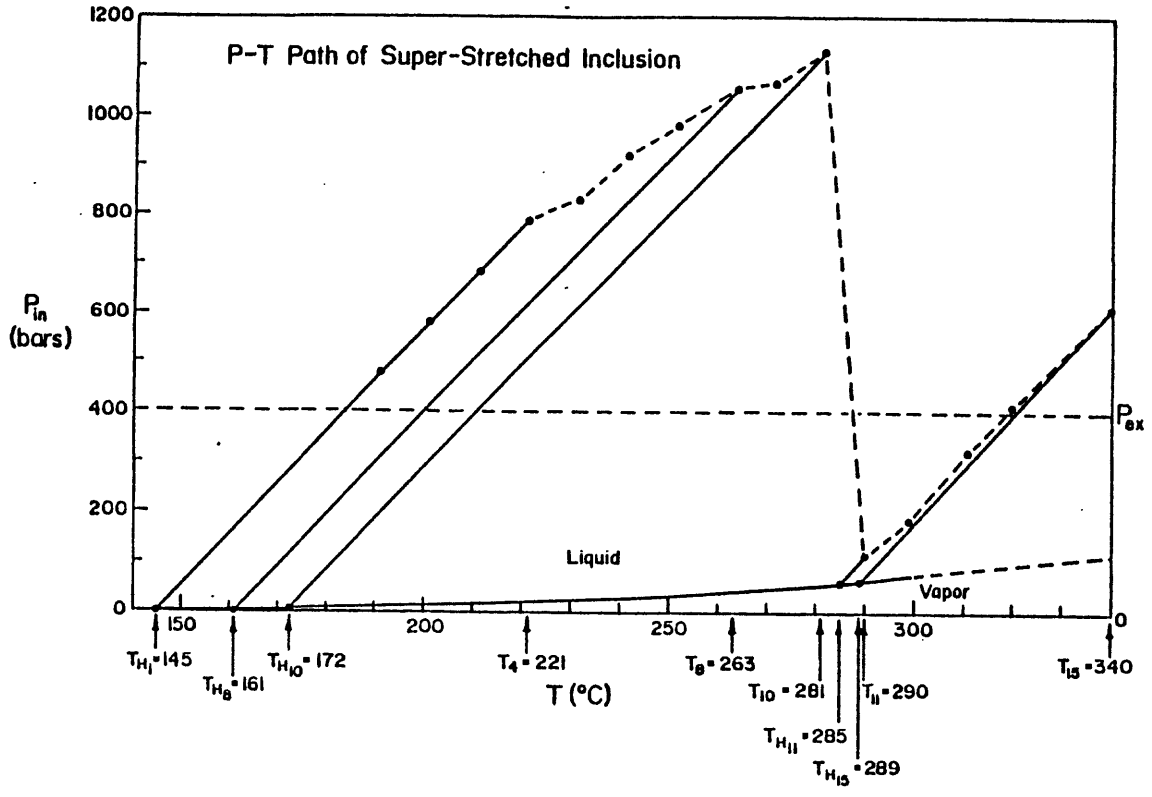

Figure 17. P-T path of a super-stretched inclusion

The path in P-T space during overheating, stretching, and super-stretching is shown for inclusion 10A-c. The stretching path for this inclusion is similar to the paths shown in figures 10 and 13 except that above a certain temperature and internal pressure (281°C, 1138 bars) this inclusion undergoes super-stretching, a volume increase great enough to lower the internal pressure. This drop in internal pressure corresponds to a sharp increase in T_H (see figure 19) and in volume (figure 15). Above 290°C stretching continues at approximately the previous rate. T_{Hi} is the initial T_H and each numbered T_H value (e.g. $T_{H\ 10}$=172°C) is the result of overheating to the indicated temperature (e.g. T_{10}=281°C). The salinity of inclusion 10A-c was 4.18 molal or 19.62 weight % NaCl equivalent, giving an isochoric slope of 10.3 bars°C; $T_{H(initial)}$ was 145° and log inclusion volume (microns)^3, 2.95. The external pressure was 400 bars.

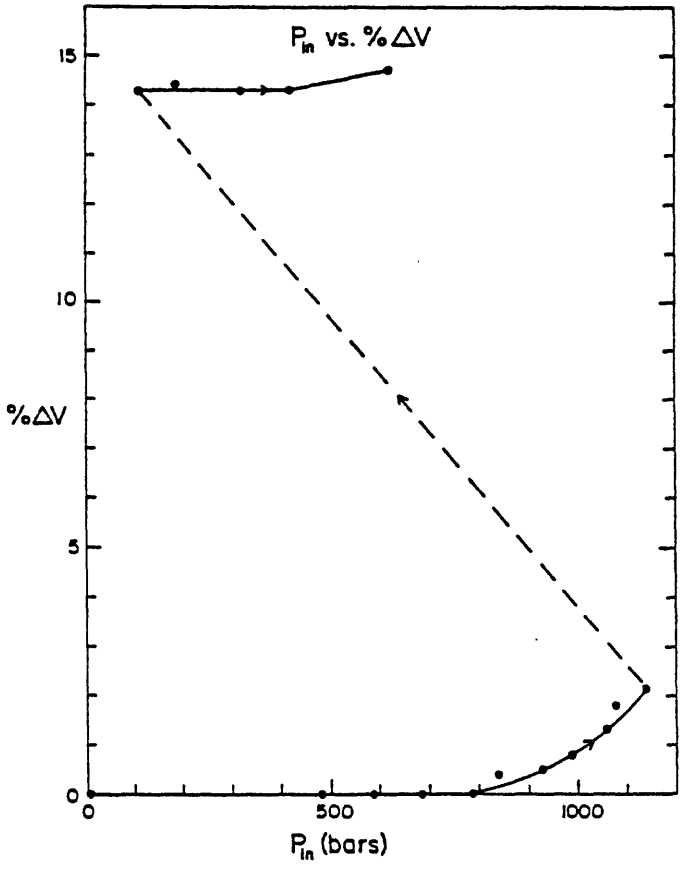

Figure 18. $P_{internal}$ vs. % volume change for a super-stretched inclusion

Pressure inside inclusion 10A-c, P_{in}, is plotted against the % increase in inclusion volume as a result of stretching. Below 793 bars internal pressure, stretching has not yet begun and there is no change in inclusion volume. Between 793 and 1138 bars stretching proceeds 'normally' with a smooth increase in volume (compare figure 16). At approximately 1138 bars, however, a rapid increase in volume associated with super-stretching causes a marked decrease in internal pressure. With continued overheating $P_{internal}$ builds and volume begins gradually to increase again (figure 17). Inclusion 10A-c was overheated at 400 bars external pressure. Its salinity was 4.18 molal or 19.62 weight % NaCl equivalent, giving an isochoric slope of 10.3 bars/°C; $T_{H(initial)}$ was 145°C and log inclusion volume (microns)^3, 2.95.

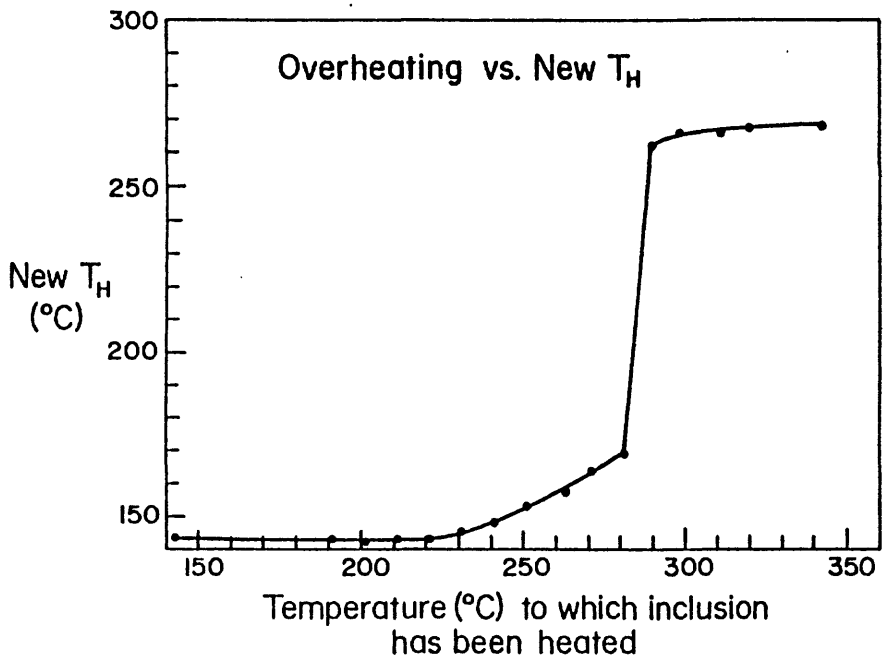

Figure 19. Overheating vs. new T_H for a super-stretched inclusion

New homogenization temperatures for inclusion 10A-a are plotted as a function of successively higher overheating temperatures. Below 221°C no stretching has occurred and T_H is at its initial value. Between 221° and 281°C overheating causes a relatively smooth increase in T_H representing the 'normal' phase of stretching (see also figures 15 and 17). Between 281° and 290°C there is an abrupt increase in T_H corresponding to super-stretching. Above 290°C overheating causes gradual continued increase in the new T_H values. Inclusion 10A-a was overheated at P_{ex}=400 bars. Its salinty was 4.18 molal or 19.62 weight % NaCl equivalent, giving an isochoric slope of 10.3 bars/°C; $T_{H(initial)}$ was 143°C, and inclusion volume $(microns)^3$, 2.82.

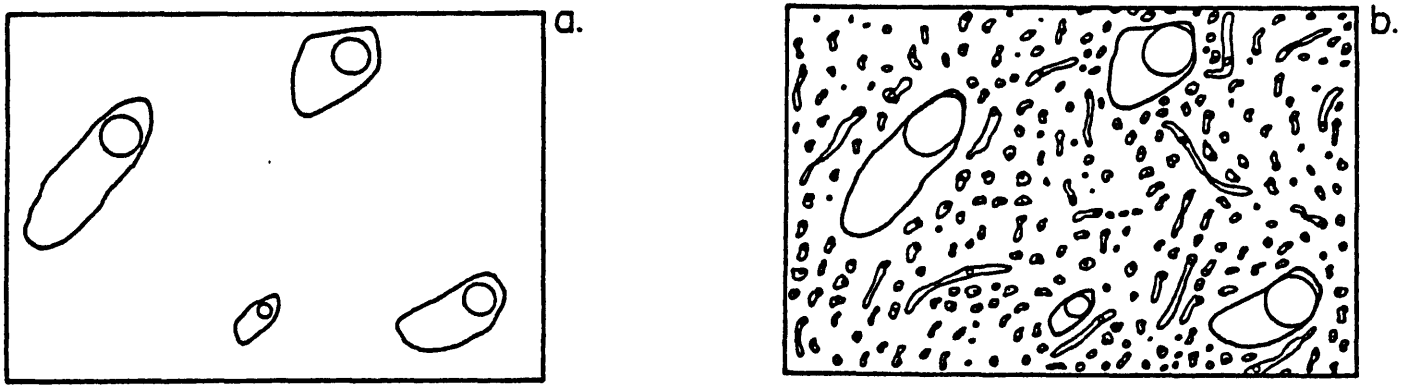

Figure 20. Inclusions before and after stretching

Fig. a. shows a group of secondary inclusions as they would appear before stretching; and Fig. b. shows the same group of inclusions after super-stretching. The high internal pressure during stretching is believed to have opened a fracture in the plane of the secondaries. Fluid that leaked from the original inclusions would have been trapped as the fracture healed during cooling, forming new daughter inclusions. Whatever the formation mechanism, tiny new inclusions are observed around the original, now super-stretched inclusions. The vapor bubbles of the super-stretched inclusions are greatly enlarged due to increased inclusion volume, decreased internal pressure, and a presumably smaller quantity of fluid.

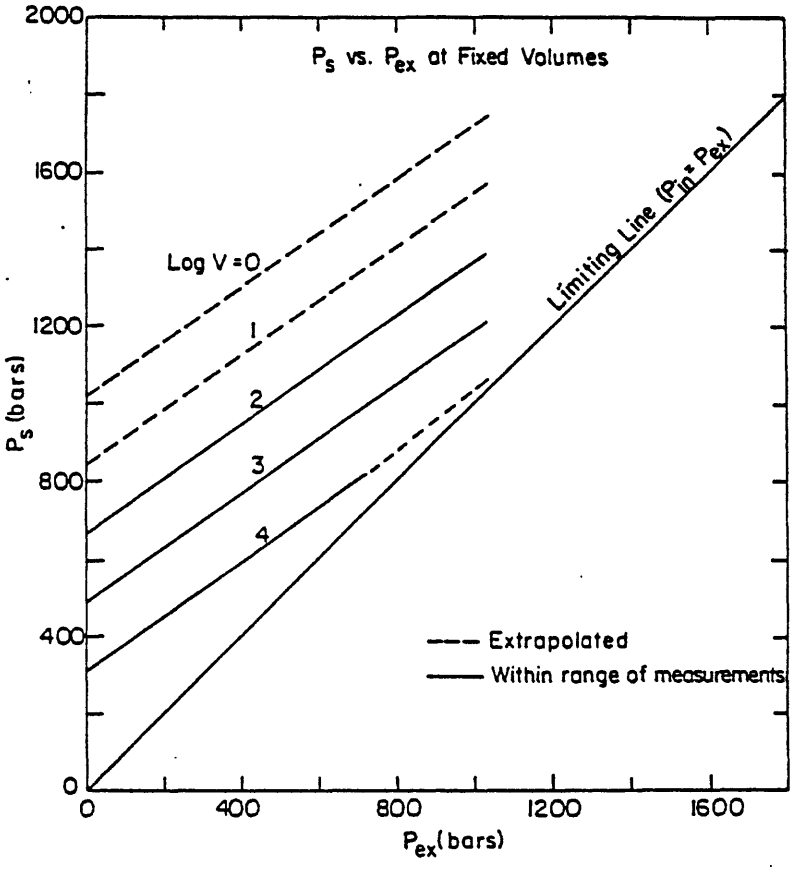

Figure 21. P_s vs. P_{ex} at fixed volumes

P_s vs. P_{ex} curves derived from the equation (2),

$$P_s = -178.0\text{LogV} + 0.7P_{ex} + 1018.9,$$

have been drawn for five inclusion volumes. The solid lines lie within the experimental P_{ex} and volume range, and dashed lines are extrapolated. Units of volume are cubic microns and the smallest inclusion used had a log volume of 1.92. The line LogV=0 represents a theoretical maximum yield strength for inclusions in fluorite. The 'limiting line', P_{in}=P_{ex}, has a slope of 1.0; below this line P_{ex} exceeds P_{in} and stretching, in the sense defined in this study, cannot occur. The isovolume curves may approach the 'limiting line' asymptotically.

temperature, and volume range of this study, breaks down as the isovolume curves approach the 'limiting line'. It is possible that the curves approach the 'limiting line' asymptotically.

No data were collected above 1034 bars external pressure because, for reasons not fully understood, T_Hs dropped instead of increasing. Inclusions left overnight at room temperature and 2 kbars water pressure showed no change in T_Hs. However, inclusions heated to their homogenization temperatures for less than an hour at 2 kbars water pressure and cooled showed decreases in T_H in the vicinity of 10°C. This phenomenon seems to be associated with the combination of high P_{ex} and cooling from elevated temperature. A similar set of experiments by James Grunig (reported in Kennedy, 1950) gave essentially the same results: T_H dropped approximately 10°C when inclusions in fluorite were subjected to 1500 bars water pressure at 150°C. It should be noted that up to about 1 kbar in this study, external pressures exceeding internal pressures had no observed effect on T_H.

Stress and temperature versus strain

In addition to providing information on the behavior of fluid inclusions, experiments such as those of the present study have been recognized as a new way of determining the tensile strength of fluorite (Sabouraud, 1981). Internal pressure is a stress exerted on the cavity walls which yield very slightly in the elastic range below P_s. Above P_s the elastic limit has been exceeded and permanent deformation or strain in the form of an inclusion volume increase results. Figure 18 shows stress (P_{in}) versus strain (% volume change) in an indivudual inclusion. Because elastic deformation is not visible at this scale, internal pressure rises vertically to the yield strength of the fluorite at 793 bars. The cavity walls yield steadily until, at an internal pressure of 1138 bars, the tensile strength of the fluorite has been reached. The internal pressure at which super-stretching takes place is the breakdown pressure, or pressure at which tensile cracks begin to propagate away from the inclusion into the crystal. Although the applied stress at failure is sometimes referred to in the literature as the strength of a material, strictly speaking, further calculations are required to translate the breakdown pressure to a tensile strength for fluorite (C. Barton, pers. comm., 1982). Above 1138 bars, brittle failure of the cavity walls causes a major volume increase from 2.15% to 14.26% over the original volume and P_{in} drops markedly. As overheating continues, P_{in} builds again and volume begins to increase slowly. Figure 15 is a similar graph showing the percent volume change with the temperature to which the inclusions were overheated. Only 18 of the 95 inclusions examined could be considered clear examples of super-stretching; their calculated breakdown pressures at 400 bars external pressure ranged from 1106 to 1442 bars, from 1503 to 1639 bars at 717 bars external pressure, and from 1964 to 2237 bars at 1034 bars external pressure. These values compare with (dry) 'rupture' strength reported by Handin (in Clark, 1966, p. 277) of 1230 to 4350 bars varying with sample geometry. The presence of water commonly has a significant effect, increasing the strength of some minerals, e.g., halite, and weakening others such as gypsum or quartz (Robertson, 1955). For quartz, water has been shown to increase dislocation mobility, and to decrease fracture toughness, i.e., resistance to crack propagation (Atkinson, 1979). Although the effect of water on dislocation mobility and fracture toughness is not known for fluorite, it should be noted when comparisons are made, that the walls of an inclusion are in contact with fluid, whereas conditions in many laboratory experiments where stress is applied mechanically are dry.

SUGGESTIONS FOR FUTURE STUDY

An extension of the P_s-P_{ex}-LogV relationship to other minerals, calcite, sphalerite, quartz, feldspars, and olivine to name a few, would perhaps be of most practical value to researchers using, or potentially using fluid inclusions in the study of mineral deposit genesis. Work by Tugarinov and Naumov (1970) relating the Mohs hardness of a mineral to the internal pressure corresponding to mass decrepitation (figure 22) suggests that the relationship defined for fluorite may be similar for other minerals, but may shift up or down depending on the strength, hardness, and cleavability of the individual mineral. Comparison of the relationship between P_s and LogV at 1 bar external pressure for fluorite and sphalerite has been examined in detail by Bodnar and Bethke (1984).

An important step in understanding the stretching mechanism would be a detailed comparison by TEM of sections cut to intersect fluid inclusions, both stretched and unstretched. The density and type of dislocations surrounding and intersecting the inclusion walls could provide key information on the importance of dislocations in the stretching process. Only brief reconnaissance examinations of this type have been made so far because ionization by the electron beam of the TEM rapidly damages the fluorite crystal obscuring the field of view. A more detailed study would probably be successful using a special low temperature TEM to minimize sample damage.

A better understanding of the behavior of fluid inclusions in fluorite at external pressures above 1 kb would be of practical value as well as potentially important to understanding the stretching mechanism. Use of very slow cooling rates, with care taken to maintain internal pressure only slightly below external during cooling, might forestall the decreases in T_H and permit extension of the present relationship to higher pressures.

SUMMARY OF CONCLUSIONS

The principal result of this study is the equation relating P_s to P_{ex} and V. With information on the volume, fluid composition, and T_H of an inclusion, and with estimates of the maximum temperature and minimum confining pressure to which inclusions may have been exposed, this relationship,

$$P_s = -178.0\text{LogV} + 0.7P_{ex} + 1018.9, \qquad (2)$$

can be used to determine whether inclusions greater than a given volume have stretched. In cases where recognition of stretching is possible based on a relationship between T_H and volume, the function $P_s=f(\text{LogV}, P_{ex})$ permits, given a confining pressure, estimates of the temperatures that resulted in stretching.

Fluid inclusions are a valuable tool in the study of mineral deposit genesis, but the temperature information they yield must be used with great discretion. Very misleading T_Hs and formation temperatures can be obtained if stretching or leakage go undetected. Leakage is commonly evident due to visible fractures around the inclusions, but stretching is a more insidious problem because it causes no visible damage to the crystal. The P_s-P_{ex}-V relationship improves the current understanding of the conditions under which stretching takes place in fluorite and improves the chances that a population of stretched inclusions will be identified. The end result, it is hoped, will be greater confidence in temperature data from fluid inclusions in the future.

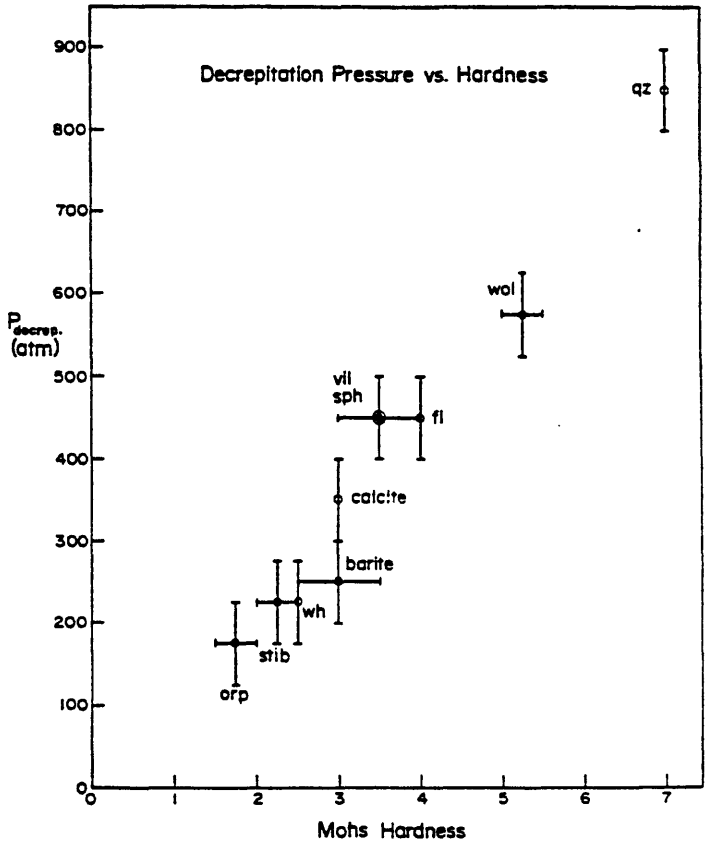

Figure 22. Decrepitation pressure vs. Mohs hardness for ten minerals (from Tugarinov and Naumov, 1970, table 2)

The internal pressure at the beginning of mass decrepitation of gas-liquid inclusions in ten minerals is shown as a function of Mohs hardness. The slope is approximately 100 to 120 atm/hardness unit. Abreviations are as follows: orp (orpiment), stib (stibnite), wh (whewellite), vil (villiaumite, sph (sphalerite), fl (fluorite), wol (wolframite), and qz (quartz).

Other results of this study have been the observation of two apparently distinct types of inclusion wall failure, first stretching, believed to be a plastic failure, followed in a few cases by super-stretching which is almost certainly a brittle failure. Finally, the fluid inclusions represent a new approach to determination of the strength of fluorite. The results of this study may ultimately contribute to the understanding of the relationship between elastic parameters, mechanisms of failure, and internal stresses necessary to initiate various levels of deformation in fluorite and other crystals.

ACKNOWLEDGMENTS

The assistance of many people has made this study possible. Philip Bethke provided the opportunity to undertake the study; continued advice and encouragement from him and Robert Bodnar have been invaluable. Consultations with others, Paul Barton and Edwin Roedder in particular, were also of great value. The experimental work was done at the U.S. Geological Survey, at Reston, Virginia. I would like to thank Philip Bethke and Julian Hemley for generously making their laboratories available. Thorough reviews by Philip Bethke, Robert Bodnar, and Edwin Roedder of the USGS in Reston, and by Professors George Brimhall and Michael Hood at the University of California, Berkeley, also made a substantial contribution to the final product. Finally, advice and ideas, as well as help with equipment and sample preparation from Nora Foley, Jim Goss, Dan Hayba, Penny Heald, and Tim Muzik are gratefully acknowledged.

The material in this open-file report was presented in 1982 as a thesis to the University of California, Berkeley, in partial fulfillment of the requirements for the degree of Master of Science.

REFERENCES

1. Atkinson, B. K. 1979, A Fracture Mechanics Study of Subcritical Tensile Cracking of Quartz in Wet Environments, Pure and Applied Geophysics, v. 117, p. 1011-1024.

2. Ballard, Stanley S., Stephen E. Brown, and James Steve Browder. 1978, Measurements of the thermal expansion of six optical materials, from room temperature to 250°C, Applied Optics, v. 17, p. 1152-1154.

3. Bodnar, R. J., and P. M. Bethke. 1984, Systematics of Stretching of Fluid Inclusions in Fluorite and Sphalerite as a Result of Overheating, ECON. GEOL., v. 79, p. 141-161.

4. Bodnar, R. J. (1983), A Method of Calculating Fluid Inclusion Volumes Based on P-V-T-X Properties of Inclusion Fluids, ECON, GEOL., v. 78, p. 535-542.

5. Bridgeman, P. W. 1928, Linear Compressibility of Fourteen Natural Crystals, Amer. J. Sci., v. 15, p. 287-296.

6. Brielles, J., and D. Vidal. 1975, Variation des Constantes elastiques de la fluorine CaF_2 avec la pression jusqu'a 12 kbar, High Temperatures-High Pressures, v. 7, p. 29-33.

7. Clynne, Michael A., and Robert W. Potter. 1977, Freezing Point Depressions of Synthetic Brines, Geol. Soc. Amer., Abs. with Prog., v. 9, p. 930.

8. Cunningham, Charles G. and Allen V. Heyl. 1980, Fluid Inclusion Homogenization Temperatures Throughout the Sequence of Mineral Deposition in the Cave-in-Rock Area, Southern Illinois, ECON. GEOL., v. 75, p. 1226-1231.

9. Freas, Donald H. 1961, Temperatures of Mineralization by Liquid Inclusions, Cave-in-Rock Fluorspar District, Illinois, ECON. GEOL., v. 56, p. 542-556.

10. Ganesan, S., and R. Srinivasan. 1959, Specific Heat and Thermal Expansion of Fluorspar, Natl. Inst. of Sci. of India--Proceedings, Pt. A, Physical Sciences, v. 25, p. 139-153.

11. Gibbard, H. Frank, and Allan R. Grossmann. 1974, Freezing Points of Electrolyte Mixtures, I. Mixtures of Sodium Chloride and Magnesium Chloride in Water, Jour. of Sol. Chem., v. 3, p. 385-393.

12. Haas, John L. 1971, The Effect of Salinity on the Maximum Thermal Gradient of a Hydrothermal System at Hydrostatic Pressure, ECON. GEOL., v. 66, 940-946.

13. Haas, John L. 1976, Physical Properties of the Coexisting Phases and Thermochemical Properties of the H_2O Component in Boiling NaCl Solutions, U. S. Geol. Survey Bull. 1421-A.

14. Hall, Wayne E. and Irving Friedman. 1963, Composition of Fluid Inclusions, Cave-in-Rock Fluorite District, Illinois, and Upper Mississippi Valley Zinc-Lead District, ECON. GEOL., v. 38, p. 886-911.

15. Handin, John. 1966, Strength and Ductility, in S. P. Clark, ed., Handbook of Physical Constants, Geol. Soc. Amer., Mem. 97, p. 223-289.

16. Hollister, L.S., et al. 1981, Practical Aspects of Microthermometry, in L. S. Hollister and M. L. Crawford, eds., Short Course in Fluid Inclusions: Applications to Petrology, Mineralogical Association of Canada, p. 278-304.

17. Ingerson, Earl. 1947, Liquid Inclusions in Geologic Thermometry, Am. Mineralogist, v. 32, p. 375-388.

18. Kennedy, George C. 1950, "Pneumatolysis" and the Liquid Inclusion Method of Geologic Thermometry, ECON. GEOL., v. 45, p. 533-547.

19. Larson, L. T., J. D. Miller, J. E. Nadeau, and E. Roedder. 1973, Two Sources of Error in Low Temperature Inclusion Homogenization Determination, and Corrections on Published Temperatures for the East Tennessee and Laisvall Deposits, ECON. GEOL., v. 68, p. 113-116.

20. Lemmlein, G. C. 1956, Formation of Fluid Inclusions in Minerals and Their Use in Geological Thermometry, Geochemistry, no. 6, p. 630-642.

21. Leroy, Jacques. 1979, Contribution a l'etalonnage de la pression interne des inclusions fluides lors de leurs decrepitation, Bull. Mineral., v. 102, p. 584-593.

22. McGee, Kenneth A., N. J. Susak, A. J. Sutton, and J. L. Haas. 1981, The Solubility of Methane in Sodium Chloride Brines, U. S. Geological Survey, Open-File Report 81-1294.

23. Pashkov, Yu. N., and G. O. Piloyan. 1973, On the Theory of the Decrepitation Method, Abstracts of Papers at the Fourth Regional Conference on the Thermobarogeochemistry of Mineral-Forming Processes, 24-30 Sept., Rostov, Rostov Univ. Press, p. 292-293. (English abstract in Proceedings of COFFI, E. Roedder, ed., v. 6, 1973, p. 119.)

24. Potter, Robert W., and David L. Brown. 1977, The Volumetric Properties of Aqueous Sodium Chloride Solutions from 0° to 500°C at Pressures up to 2000 Bars Based on a Regression of Available Data in the Literature, U. S. Geol. Survey Prof. Bull. 1421-C.

25. Potter, Robert W., and Michael A. Clynne. 1978, Pressure Correction for Fluid Inclusion Homogenization Temperatures, Prog. and Abs., Int. Assoc. on the Genesis of Ore Deposits Symposium, Snowbird, Alta, Utah.

26. Potter, Robert W., Michael A. Clynne, and David L. Brown. 1978, Freezing Point Depression of Aqueous Sodium Chloride Solutions, ECON. GEOL., v. 73, p. 284-285.

27. Richardon, C. K. and H. D. Holland. 1979, Fluorite Deposition in Hydrothermal Systems, Geochim. et Cosmochim. Acta, v. 43, p. 1327-1335.

28. Robertson, Eugene C. 1955, Experimental Study of the Strength of Rocks, Geol. Soc. Amer. Bull., v. 66, p. 1275-1314.

29. Roedder, Edwin. 1962a, Studies of Fluid Incluions I: Low Temperature Application of a Dual Purpose Heating and Freezing Stage, ECON. GEOL., v. 57, p. 1045-1061.

30. Roedder, Edwin. 1962b, Ancient Fluids in Crystals, Scientific American, v. 207, p. 38-47.

31. Roedder, Edwin. 1965, Liquid CO_2 Inclusions in Olivine-Bearing Nodules and Phenocrysts from Basalts, Am. Mineralogist, v. 50, p. 1746-1782.

32. Roedder, Edwin. 1970, Application of an Improved Crushing Microscope Stage to Studies of the Gases in Fluid Inclusions, Schweiz. Mineralogische und Petrographische Mittellungen, v. 50/1.

33. Reodder, Edwin. 1972, The Composition of Fluid Inclusions, Chapter JJ in M. Fleischer, ed., Data of Geochemistry, 6th ed., U. S. Geol. Survey Prof. Paper 440.

34. Roedder, Edwin. 1981, Origin of Fluid Inclusions and Changes that Occur after Trapping, in L. S. Hollister and M. L. Crawford, eds., Short Course in Fluid Inclusions: Applications to Petrology, Mineralogical Association of Canada, p. 101-137.

35. Roedder, E., B. Ingram, and W. E. Hall. 1963, Studies of Fluid Inclusions: III. Extraction and Quantatative Analysis in the Milligram Range, ECON. GEOL., v. 58, p. 353-374.

36. Roedder, Edwin, and Brian J. Skinner. 1968, Experimental Evidence that Fluid Inclusions do not Leak, ECON. GEOL., v. 63, p. 715-730.

37. Sabouraud, Christiane. 1981, Decrepitation Experimentale d'Inclusions sous Pression. Application au Cas d'Inclusions Primaires de Fluorine, Acad. Sc. Paris, C. R. Hebd., t. 292, p.729-732.

38. Saylor, Charles P. 1965, A Study of Errors in the Measurement of Microscopic Spheres, Applied Optics, v. 4, p. 477-486.

39. Sharonov, B. N., Yu. V. Lir, and A. V. Kozlov. 1973, On the Question of Interpretation of Decrepigraphs of Vein Quartz, Abstracts of Papers at the Fourth Regional Conference on Thermobarogeochemistry of the Mineral-Forming Processes, 24-30 Sept., Rostov, Rostov Univ. Press, p. 309-311. (English abstract in Proceedings of COFFI, E. Roedder, ed., v. 7, 1974, p. 203-204.)

40. Shatagin, N.N. 1973, Dependence of Decrepitation Temperature on Size of Inclusions, Thickness of Inclusion Wall, and Pressure of Mineral-Formation, Abstracts of Papers at the Fourth Regional Conference on Thermobarogeochemistry of Mineral-Forming Processes, 24-30 Sept., Rostov, Rostov Univ. Press, p. 293-295. (English abstract in Proceedings of COFFI, E. Roedder, ed., v. 7, 1974, p. 204.)

41. Skinner, Brian J. 1966, in S. P. Clark, ed., Handbook of Physical Constants, Geol. Soc. Amer., Mem. 97, p. 75-96.

42. Stephenson, T. E. 1952, Sources of Error in the Decrepitation Method of Study of Liquid Inclusions, ECON. GEOL., v. 47, p. 743-750.

43. Susak, N. J., and K. A. McGee. 1980, A Routine for Estimating the Solubility of Methane in Pure Water or NaCl Brines by Using the Texas Instruments TI-59 Calculator-With Tables, U. S. Geological Survey, Open-File Report 80-371.

44. Tugarinov, A.I., and V.B. Naumov. 1970, Dependence of the Decrepitation Temperature of Minerals on the Composition of their Gas-Liquid Inclusions and Hardness, Doklady Akad. Nauk SSSR, v. 195, p. 112-114.

45. Vaidya, S. N., S. Bailey, T. Pasternack, and G. C. Kennedy. 1973, Compressibility of Fifteen Minerals to 45 Kilobars, Jour. Geophys. Res., v. 78, p. 6893-6898.

46. Vidal, M. Daniel. 1974, Physique des Solides-Mesure des constantes du fluorure de calcium monocristallin de 20° a 850°C, Acad. Sc. Paris, C. R. Hebd., t. 279, p. 345-347.

47. Werre, R.W., R.J. Bodnar, P.M. Bethke, and P.B. Barton. 1979, A Novel Gas-Flow Fluid Inclusion Heating/Freezing Stage, Geol. Soc. Amer., Abs. with Prog., v. 11, p. 539.

48. Wong, C., and D. E. Schuele. 1968, Pressure and Temperature Derivatives of the Elastic Constants of CaF_2 and BaF_2, Jour. Phys. Chem. Solids, v. 29, p. 1309-1330.

Appendix A

Calculation of Inclusion Volumes

In any fluid inclusion study it is useful to be able to find inclusion volumes. A new method developed by Robert Bodnar (1983) relies only on a knowledge of the P-V-T-X properties of the inclusion fluid and on the volume of the vapor phase at a given temperature. Where the vapor bubble is assumed spherical, the only measurement involved is that of the vapor bubble diameter; the vapor phase volume is then easily computed. For an inclusion which homogenizes to a liquid phase the method can be stated as follows:

$$\%\ \text{change in}\ V_{sp}(\text{liquid})\ X\ V(\text{total inclusion}) = V(\text{vapor bubble})$$

The first term represents the percent change in specific volume of the liquid between room temperature and T_H, relative to the specific volume at T_H. Given the density data for the fluid, this term is simply $\{d^{-1}(T_H) - d^{-1}(25°)\}\ /d^{-1}(T_H)$, where specific volume (d^{-1}) is the inverse of density, d. Vapor bubble volume is computed from the diameter measured at room temperature and the equation is solved for the total inclusion volume.

This method is based on the assumption that the inclusion is an isolated system, with the mass of the inclusion contents and the total volume fixed. Homogenization (to a liquid phase) represents the point where the liquid has expanded to fill the entire cavity, therefore the liquid at T_H has lower density and higher specific volume than at room temperature. The percent change in specific volume multiplied by the total inclusion volume gives the amount of expansion of liquid in absolute volume units. Since the liquid expands at the expense of the shrinking vapor bubble which vanishes at T_H, the vapor bubble volume must exactly equal the amount of the liquid's expansion.

Inclusion volumes can also be determined by measuring the dimensions of an inclusion, and computing the volume of the closest geometric form of the same dimensions. The main drawbacks of this method are (1) that the choice of usable inclusions is severely limited because the method is applicable only to inclusions of very regular shape, and (2) since the third dimension cannot be measured it must be estimated, introducing error of unknown size. Comparisons of volumes of regularly shaped inclusions computed by each method showed good agreement indicating that either method is satisfactory for these inclusions (Bodnar and Bethke, 1984). For irregualrly shaped inclusions however, the Bodnar method provides the best volme estimates available.

There are a number of sources of error in the Bodnar method, the most significant of which is the accuracy of the computed vapor bubble volume. The bubble diameter is measured using a calibrated ocular micrometer with a precision of ± 0.5 microns and this may represent substantial error when the radius is cubed to get the vapor phase volume. These errors are directly proportional to errors in total inclusion volume so that a vapor bubble volume 10% too high would yield a total volume 10% too high as well. There are also difficulties inherent in the accurate microscopic measurement of spheres. The refractive index of the medium surrounding the sphere, the focal position, condenser aperture and position all influence the apparent diameter to some degree (Saylor, 1965). In addition, Roedder (1972, Plate 11, figs. 7, 8) has shown that a curved inclusion wall may act as a negative lens distorting the apparent diameter of the vapor bubble. This problem becomes less serious as the refractive index of the host mineral approaches that of the inclusion fluid. Compared with a high index mineral such as sphalerite (n=2.37) the index of fluorite, 1.43, is relatively close to the index of the fluid,

approximately 1.10. Finally, it should be pointed out that the vapor bubbles could not be true spheres unless they floated in the liquid. Assuming that they touch one of the cavity walls, their shape will be that of a sphere slightly flattened on one side. In this study, only inclusions whose vapor bubbles showed no measurable elongation along either axis were used. These sources of error have not specifically been taken into account because they are believed to be far outweighed by the uncertainty in the vapor bubble diameter measurement.

APPENDIX B

Data Tables

Table 1. Multiple Regression Input. Data for 141 secondary inclusions are listed; all data at P_{ex}=1 bar are from Bodnar and Bethke (1984).

Inclusion Number	P_s	LogV	P_{ex}	Inclusion Number	P_s	LogV	P_{ex}
A1	505	3.32	1	P2	644	2.20	1
A2	657	1.68	1	P3	652	1.68	1
A3	585	2.58	1	P4	697	1.97	1
A4	477	2.58	1	X1	185	4.91	1
A5	567	2.58	1	X2	104	4.54	1
A6	482	2.88	1	X3	266	4.68	1
A7	477	3.11	1	X4	188	4.54	1
A8	454	3.32	1	X6	268	4.54	1
A9	482	2.88	1				
A10	482	2.58	1	35-a	621	3.11	200
A11	500	3.11	1	35-b	616	3.14	200
A12	494	3.32	1	35-c	510	3.14	200
A13	485	3.11	1	35-e	609	3.08	200
K1	333	3.11	1	35-f	520	3.33	200
K2	390	3.64	1	35-g	606	3.14	200
K3	436	2.88	1	35-h	759	2.47	200
K4	707	2.58	1	35-i	752	2.85	200
K8	230	3.32	1	35-j	713	2.51	200
K10	388	2.88	1	35-k	713	2.47	200
L1	173	4.00	1	35-l	806	2.47	200
L2	276	3.32	1	35-m	617	2.56	200
L3	475	1.68	1	35-n	662	2.78	200
L4	504	2.88	1	35-o	814	2.47	200
L5	516	2.58	1	35-p	474	3.03	200
L7	432	3.49	1	35-q	661	2.88	200
L8	333	3.78	1	35-r	609	2.85	200
L9	425	2.88	1	35-s	622	2.47	200
L10	515	3.32	1	35-t	757	2.81	200
L11	481	2.20	1	35-u	723	1.94	200
M1	299	4.38	1	35-v	719	2.285	200
M2	317	4.20	1	35-w	711	2.81	200
M3	383	4.11	1	35-x	622	2.51	200
M4	240	3.78	1	35-y	765	2.47	200
M5	233	4.46	1	35-z	760	2.51	200
M6	312	4.11	1	35-aa	710	2.85	200
M7	276	4.54	1	35-bb	813	2.47	200
P1	644	2.20	1	35-cc	812	2.23	200

Table 1. (Cont.)

Inclusion Number	P_s	LogV	P_{ex}	Inclusion Number	P_s	LogV	P_{ex}
9A-b	682	3.89	400	32-o	1002	2.81	717
9E-a	768.5	3.23	400	32-p	1114	2.51	717
9E-d	705	3.13	400	32-q	1123	2.60	717
9E-f	609	3.23	400	32-r	1113	2.51	717
10A-a	750.5	2.82	400	32-s	863	2.84	717
10A-b	846	3.00	400	32-t	999	2.78	717
10A-c	837	2.95	400	32-u	922	3.11	717
10A-d	1056	1.92	400	32-v	997	2.67	717
10A-e	842	2.68	400	32-w	1060	2.56	717
10A-f	851	2.88	400	32-x	1118	2.47	717
10A-g	843	3.26	400	32-y	996	2.81	717
10A-h	853	2.95	400	32-z	1223	2.07	717
12B-a	1003	2.27	400				
12B-b	887	2.90	400	21A-a	1261	3.07	1034
12B-c	882	2.84	400	21A-b	1138	3.07	1034
12B-d	881	2.55	400	21A-c	1370	1.97	1034
12B-e	879	2.55	400	21A-d	1474	2.23	1034
12B-f	1093	2.37	400	21A-e	1285	2.23	1034
12B-g	1104	1.93	400	21A-f	1287	2.45	1034
12B-i	1106	2.06	400	21B-g	1290	2.23	1034
				21B-h	1133	2.63	1034
32-a	919	3.33	717	21B-i	1275	2.80	1034
32-b	990	2.78	717	21B-j	1039	3.40	1034
32-c	1113	2.81	717	21B-k	1154	2.80	1034
32-d	1111	2.51	717	21B-l	1143	2.94	1034
32-e	1116.5	2.56	717	21B-m	1141	2.94	1034
32-f	1212	1.94	717	21B-o	1270	2.63	1034
32-g	1067	2.81	717	22-a	1384	1.97	1034
32-h	995.5	2.84	717	22-b	1394	2.11	1034
32-i	1175	2.07	717	22-c	1410	2.23	1034
32-j	994	2.56	717	22-d	1144	2.80	1034
32-k	994	2.63	717	22-e	1228	2.34	1034
32-l	998	2.63	717	22-f	1484	2.34	1034
32-m	1224	1.94	717	22-g	1258	2.94	1034
32-n	1118	2.60	717	22-h	1125	3.54	1034

Table 2. Statistics from (SPSS) Multiple Regression of the data gathered for 141 secondary inclusions (see Table 1.).

Dependent Variable	P_s
Sample Size	141
Multiple Correlation Coefficient	0.97139
Standard Deviation	79.51453

Variable Name	Value	Standard Error	F Statistic	Significance Level of F
LogV	-177.99162	10.998620	261.89228	.000
P_{ex}	.70512190	.019038850	1371.6616	0
Constant	1018.9445	35.307778	832.83748	0

Table 3. Data for Inclusion 10A-c, used in plotting figures 15,17, and 18. Inclusion 10A-c was overheated at P_{ex}=400 bars. Salinity: 4.18 molal or 19.62 weight % NaCl equivalent; isochoric slope: 10.3 bars/°C; $T_{H(initial)}$: 145°C; log inclusion volume (microns)^3: 2.95.

No.	T_{OH} (°C)	T_H (°C)	D (gm/cc)	V_{sp} (cc/gm)	$(V-V_O)/V_O$	P_{in} (bars)
initial	145	145.0	1.065	.939	0	4
1	191	145.0	1.065	.939	0	484
2	201	145.0	1.065	.939	0	587
3	211	145.0	1.065	.939	0	690
4	221	145.0	1.065	.939	0	793
5	231	150.8	1.060	.943	.443	836
6	241	151.6	1.059	.944	.505	932
7	251	155.6	1.056	.947	.818	994
8	263	161.4	1.051	.951	1.280	1058
9	271	167.8	1.046	.956	1.803	1078
10	281	172.0	1.042	.959	2.153	1138
11	290	285.4	.932	1.073	14.256	107
12	299	286.8	.930	1.075	14.443	189
13	311	285.8	.931	1.074	14.309	323
14	320	285.7	.932	1.073	14.296	416
15	342	288.5	.929	1.077	14.672	616

Table 4. Data for Inclusion 32-a, used in plotting figures 13 and 16. Inclusion 32-a was overheated at P_{ex}=717 bars. Salinity: 4.414 molal or 20.51 weight % NaCl equivalent; isochoric slope: 10.5 bars/°C; $T_{H(initial)}$=145°C; log inclusion volume: 3.33.

No.	T_{OH} (°C)	T_H (°C)	D (gm/cc)	V_{sp} (cc/gm)	$(V-V_O)/V_O$	P_{in} (bars)
initial	145	145	1.071	.933	0	4
1	221	145	1.071	.933	0	803
2	232	145	1.071	.933	0	919
3	245	148	1.069	.935	.224	1024
4	255	150.5	1.067	.937	.413	1103
5	265	153	1.065	.939	.604	1182
6	278	156	1.062	.941	.835	1288
7	289	164	1.056	.947	1.466	1321
8	301	171	1.050	.952	2.034	1375
9	315	176	1.046	.956	2.450	1470
10	328	187	1.036	.965	3.393	1493
11	341	196	1.028	.972	4.196	1537
12	353	204.5	1.021	.980	4.981	1576
13	367	214	1.012	.988	5.891	1628
14	380	226	1.000	1.000	7.090	1642
15	390	234	.993	1.007	7.921	1667

Table 5. Data for inclusion 10A-a, used in plotting figure 19. Inclusion 10A-a was overheated at 400 bars external pressure. Salinity: 4.18 molal or 19.62 weight % NaCl equivalent; isochoric slope: 10.3 bars/°C; $T_{H(initial)}$=143°C; log inclusion volume: 2.82.

No.	T_H (°C)	T_{OH} (°C)
initial	143	143
1	143	191
2	142	201
3	143	211
4	143	221
5	145	231
6	148	241
7	153	251
8	157	263
9	164	271
10	169	281
11	262	290
12	266	299
13	266	311
14	267	320
15	268	342